Magazine of Civil Engineering

ISSN 2712-8172

journal homepage: http://engstroy.spbstu.ru/

Research article

UDC 624.13

DOI: 10.34910/MCE.141.2

Dynamic characteristics of machine foundation under harmonic loading on gypseous soil with various degrees of saturation

M.Y. Fattah[1], ***A.S. Abood***[1], ***M.M. Sabri***[2,3] ✉, ***A.Sh. Al-Adili***[1]

[1] *College of Civil Engineering, University of Technology, Baghdad, Iraq*

[2] *Peter the Great St. Petersburg Polytechnic University, St. Peterburg, Russian Federation*

[3] *Moscow Automobile and Road Construction State Technical University (MADI), Moscow, Russian Federation*

✉ *mohanad.m.sabri@gmail.com*

Keywords: amplitude, dynamic behavior, dynamic characteristics, gypseous soil, harmonic loading, saturation degree

Abstract. Most existing studies on collapsible soils report considerable scatter in their results, primarily due to variations in testing procedures and sampling methods. These studies have also often relied on static testing as the primary method of validation. However, as development continues, a gap remains in our understanding of how collapsible soil reacts to various dynamic stresses, including mechanical equipment, power stations, trains, roadways, and other dynamic loads. Conventional studies often fail to adequately represent real dynamic loading conditions. Accordingly, it is essential to investigate the response of gypseous soils to vibration and varying moisture content. This research aims to characterize the dynamic behavior of gypseous soil under different saturation states (unsaturated and saturated), subjected to harmonic loading at a relative density of 35 %, with additional consideration of foundation depth and eccentric mass. The experimental program aims to establish a database that enables reliable correlations between wave attenuation and soil damping in gypseous soils. Results showed that the dynamic characteristics of gypseous soil increased with frequency by approximately 50–52 % (settlement), 3–6 % (suction stress), 47–68 % (total stress), 42–46 % (acceleration), and 44–48 % (vertical displacement). With rising saturation up to 60 %, these properties decreased by 6–7 % (settlement and total stress), 2–5 % (acceleration), and 6–9 % (vertical displacement). Between 60 % and 100 % saturation, the values rose sharply, reaching 149–150 % (settlement), 139–173 % (total stress), 50–51 % (acceleration), and 52–54 % (vertical displacement). Foundation embedment from 0.0 B to 1.0 B reduced the peak dynamic responses by approximately 10 % to 15 %, whereas increasing the eccentric mass from 28 g to 44.8 g (a factor of about 1.6) amplified them by approximately 17 % to 68 %, with vertical stress and displacement showing the largest increases. Meanwhile, suction stress rose markedly (approximately 453–457 %) as saturation increased to 60 %, then fell by nearly 100 %, approaching zero, as saturation rose toward full saturation, consistent with the loss of matric suction.

Funding: This research was partially funded by the Ministry of Science and Higher Education of the Russian Federation (funding No FSFM-2024-0025).

Citation: Fattah, M.Y., Abood, A.S., Sabri, M.M., Al-Adili, A.Sh. Dynamic characteristics of machine foundation under harmonic loading on gypseous soil with various degrees of saturation. Magazine of Civil Engineering. 2026. 19(1). Article no. 14102. DOI: 10.34910/MCE.141.2

1. Introduction

Gypseous soils are widely distributed across arid and semi-arid regions, where they form a substantial portion of the surface and near-surface deposits; such soils are typically unsaturated or partially saturated, characterized by an air-water interface and a contractile skin resulting from the presence of pore water. According to [1], soil consists of air, water, and solids. However, recent research indicates that the air-water interface (or contractile skin) plays a crucial role that must be considered independently of other physical factors. The study [2] explains that when the air phase is continuous, the contractile skin interacts with soil particles, altering the mechanical behavior of unsaturated soil.

Several researchers have investigated the influence of various variables on stiffness and the material damping ratio [3–8]. The shear strain amplitude, mean effective confining stress, soil type, and plasticity index are all key factors in determining the shear modulus. Additionally, the number of loading cycles or the loading frequency plays a more critical role than the void ratio, over-consolidation ratio, grain characteristics, and degree of saturation. Other significant factors affecting the damping ratio include soil type, plasticity index, number of loading cycles, loading frequency, and shear strain amplitude [4].

The design and construction of machine foundations represent a critical component of industrial development. National investments in infrastructure and industrial facilities provide the basis for the expansion of other economic sectors, including commerce and tourism.

The foundations of machines subjected to vertical vibrations are commonly evaluated using peak acceleration as the primary control parameter for performance. Soil particles reach equilibrium at a characteristic peak acceleration that depends on the relative density of the granular soil. Further densification occurs only when this acceleration threshold is exceeded [9].

The authors [10] investigated the effects of cyclic loading on unsaturated soils using a triaxial system equipped with strain transducers for small-strain measurements and psychrometers for suction monitoring. A fixed water ratio was maintained during testing on kaolin specimens. The results indicated that suction decreased progressively with increasing number of loading cycles. Furthermore, the resilient modulus increased with rising water content up to an optimum level, beyond which it decreased sharply with further increases in water content.

The cyclic behavior of unsaturated soils was studied by the authors [11] using a triaxial test subjected to low loads and varying temperatures. Experiments have shown that under low loads, low temperatures, and high suction, the soil becomes consistently more rigid. The results of the cyclic triaxial test indicate that the soil's plasticity increases with the number of cycles, but all the unsaturated test samples reached a stable state after 100 cycles. The total plastic strain after 100 cycles was greater at higher temperatures and lower suction levels. Each result was influenced by either suction hardening or heat softening, respectively. The study also found that suction had a significant effect on the resilient modulus. The resilient modulus can increase by up to an order of magnitude when suction rises from zero to 250 kPa at a given temperature.

Physical, chemical, or combined types of weathering can break down rock components, but soil is among the most valuable natural resources produced by these processes. Soil formation in a specific location, or "zone," is heavily influenced by the region's geology, geography, and climate. Unsaturated soil is generally regarded as a three-phase system, comprising solid, liquid, and gaseous phases. Interactions among these parts, whether under static or dynamic stress, result in significant changes to the system's characteristics. Static loads remain constant over time and space, whereas dynamic loads change in direction, position, and/or amplitude. Many researchers are eager to explore the complexities of soil behavior under various dynamic loading conditions. The response of sedimentary soils to dynamic loading, such as strong earthquake motions, is significantly influenced by their dynamic properties, including stiffness degradation, modulus reduction, and damping [12]. Examples include shear wave velocity, changes in stiffness or decreasing modulus, material damping at strain levels, and components sensitive to liquefaction, all of which are extensively studied. The ability to predict or interpret dynamic behavior depends on understanding the soil's dynamic characteristics. Geotechnical earthquake engineering relies heavily on accurate estimates of dynamic soil parameters. Factors such as stress state, confinement, stress history, void ratio, water content, and other conditions influence dynamic soil properties [13].

The resilient modulus of subgrade soils has been widely investigated and is influenced by several factors, including the number of loading cycles, loading frequency, grain-size distribution, and stress history. The study [14] concluded that stress is the most critical parameter governing this behavior.

Two principal processes of soil deformation under dynamic loading are liquefaction and cyclic mobility. Both are associated with increases in pore water pressure, which reduces the effective stress and weakens soil resistance under repeated shear loading. In loose, non-cohesive, moisture-sensitive soils, particularly coarse silt and fine to medium sands, dynamic vibrations can induce liquefaction. Under such

conditions, soil grains densify, transferring intergranular stresses to the pore water. When the pore water pressure equals the total stress, the effective stress becomes zero, and the soil loses all its frictional shear strength. Liquefaction typically leads to rapid settlement and severe degradation of track or foundation geometry. Cyclic mobility, in contrast, can occur in both loose and dense soils, although liquefaction is predominantly associated with loose deposits [15].

The authors [16] experimentally demonstrated that embedment of a square footing in medium sand reduces settlement by approximately 15.2–17.3 % at a load amplitude of 0.5 t, and by 6.7–10.5 % at 1 t. In dense sand, settlement reduction reached 25.2–42.5 % at 0.5 t, 9.7–29.1 % at 1 t, and 12.6–23.2 % at 2 t.

Similarly, the authors [17] investigated contact pressure distribution beneath circular shallow foundations subjected to vertical and rocking vibration modes. Tests on dry sands of varying densities indicated that vertical settlement decreased with increasing embedment due to enhanced vertical stiffness. Under rocking vibration, stress distribution along the base increased toward the center before diminishing outward. Lateral edge strains rose from 100 % to 150 % in the rocking direction, while vertical rocking generally induced a central depression, resulting in maximum stresses beneath the footing.

Limited research has addressed the behavior of collapsible soils under vibration and repeated loading, particularly in the case of moisture-sensitive gypseous soils. To advance understanding, this study investigates the influence of repeated loading on sandy gypseous soils, with emphasis on how varying saturation levels affect key engineering properties. Factors considered include foundation type, machine characteristics, dynamic load frequency, number of load cycles, elastic modulus variation, foundation embedment, and displacement amplitude. Furthermore, the study aims to clarify the behavior of gypseous soil by analyzing the response of unsaturated samples subjected to vertical vibrations.

2. Methods

This section presents the experimental program, including soil characterization, model preparation, instrumentation, and testing procedures. The methods used for applying cyclic loads and monitoring the response of gypseous soil are described in detail to achieve the objectives of this research.

2.1. Soil Properties

The soil experiments in this paper were conducted on gypseous, collapsible soil. The soil underwent a standard set of tests to determine its physical properties. Fig. 1 displays the soil grain size distribution, and Table 1 presents some of the physical features of gypseous soil that were examined.

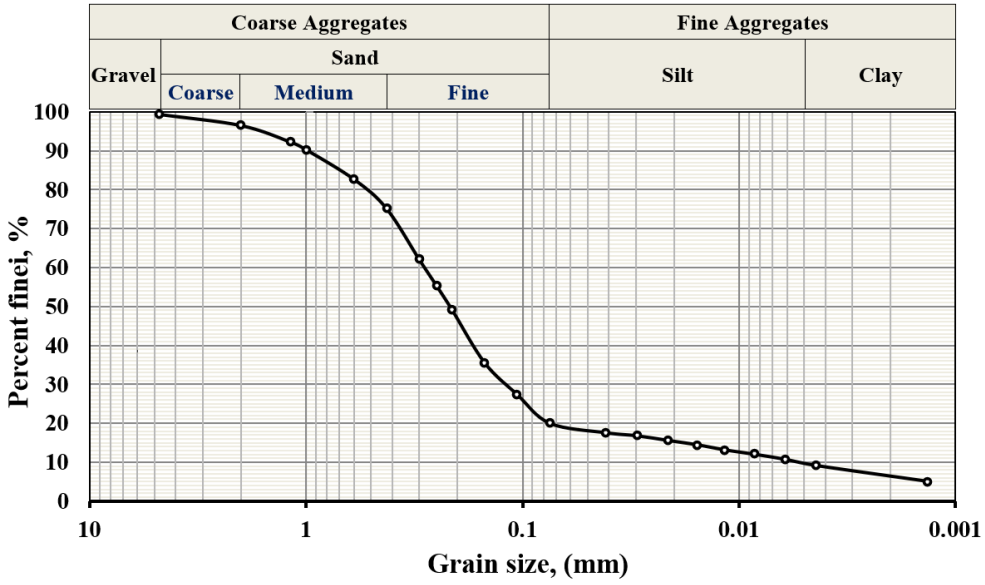

Figure 1. Grain size in the gypseous soil.

Table 1. The characteristics of the gypseous soil.

Property		Value	Reference
Specific gravity	G_s	2.43	ASTM D854[1]
Distribution of particle size, %	Fines	20	ASTM D422[2]
	Sand	79	
	Gravel	1	
Atterberg limits, %	L.L	20	ASTM D854[1]
	P.L	16	ASTM D4318[3]
	P.I	4	ASTM D4318[3]
Classification of soil	U.S.C.S	SM	ASTM D2487[4]
Min. of dry density	$\rho_{d\text{-}min}$, g/cm^3	1.20	ASTM D4254[5]
	e_{max}	1.03	
Max. of dry density	$\rho_{d\text{-}max}$, g/cm^3	1.71	ASTM D4253[6]
	e_{min}	0.42	

Additionally, the B.S. 1377[7] specification was followed to conduct a standard set of experiments necessary to determine the soil's chemical properties. The various chemical characteristics of soil are shown in Table 2 [18].

Table 2. A summary of gypseous soil's chemical characteristics.

Property	Rate of value
Gypsum content ($CaSO_4$), %	45.0
Carbonate content ($CaCo_3$), %	22.5
Total sulphate content (SO_3), %	21.07
Organic matters (O.M), %	0.72
Total soluble salts (T.S.S), %	40.1
pH value (pH)	7.23

2.2. Model tests

To investigate the behavior of gypseous soil at different saturation levels under harmonic loading and to replicate the dynamic properties of the physical model for the machine's foundation, a small-scale model was created at a 1:100 scale. Each component was carefully calibrated, and built-in measuring sensors were included. At a relative density of 35 %, 54 models were tested. Fig. 2 shows the detailed testing schedule.

[1] *ASTM D854. Standard Test Methods for Specific Gravity of Soil Solids by Water Pycnometer. ASTM International. West Conshohocken, PA, USA.*

[2] *ASTM D422. Standard Test Method for Particle-Size Analysis of Soils. ASTM International. West Conshohocken, PA, USA.*

[3] *ASTM D4318. Standard Test Methods for Liquid Limit, Plastic Limit, and Plasticity Index of Soils. ASTM International. West Conshohocken, PA, USA.*

[4] *ASTM D2487. Standard Practice for Classification of Soils for Engineering Purposes (Unified Soil Classification System). ASTM International. West Conshohocken, PA, USA.*

[5] *ASTM D4254. Standard Test Methods for Minimum Index Density and Unit Weight of Soils and Calculation of Relative Density. ASTM International. West Conshohocken, PA, USA.*

[6] *ASTM D4253. Standard Test Methods for Maximum Index Density and Unit Weight of Soils Using a Vibratory Table. ASTM International. West Conshohocken, PA, USA.*

[7] *BS 1377. Methods of Test for Soils for Civil Engineering Purposes. British Standards Institution. London, UK.*

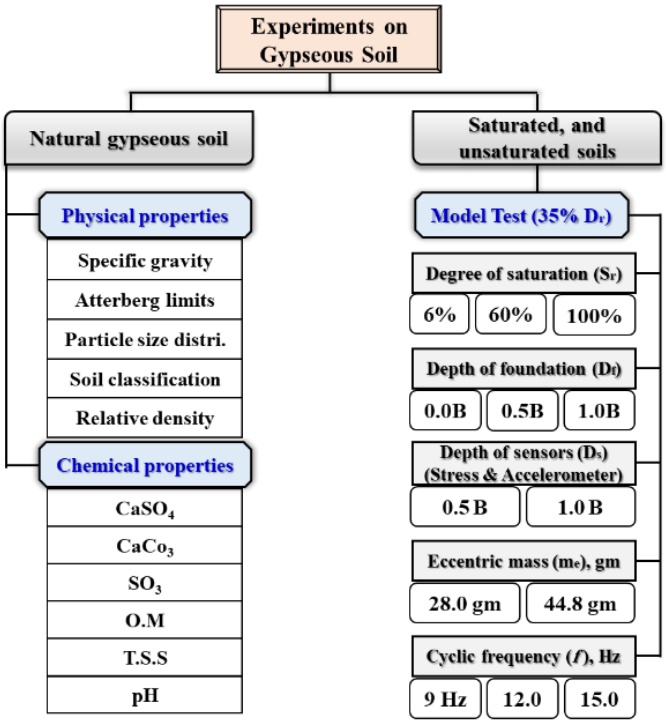

Figure 2. Testing program.

2.3. The Model and Instruments

The prototype container box has a steel plate thickness of 6 mm, with external dimensions of 500 mm by 500 mm by 570 mm. Two layers of absorbent material (each 10 mm thick) were attached to the inside surfaces of the iron box to reduce the reflection of vibration waves at the box boundaries. Each absorption layer is made from different materials (rubber and polystyrene). The steel container box used in the tests is shown in Fig. 3.

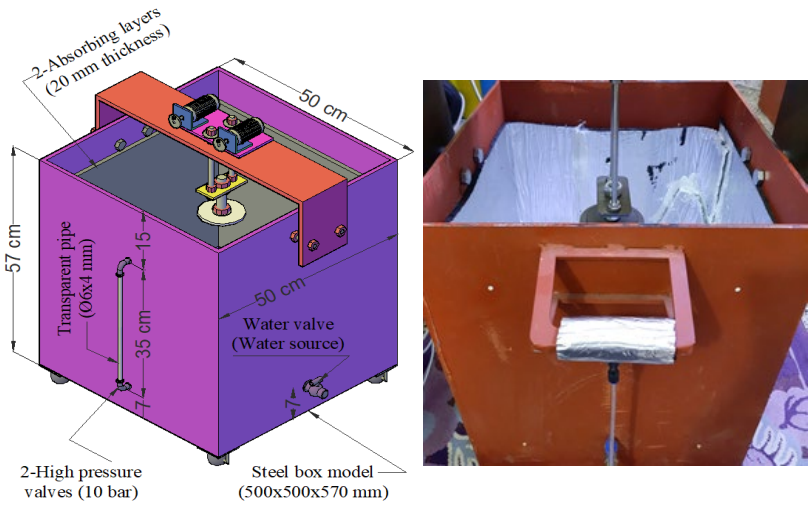

Figure 3. The steel container box.

For this purpose, a compact oscillator was built for lab testing. Also known as a 2-mass oscillator, this device is used to generate harmonic vibrations. The speed regulator panel enables the user to adjust the voltage supplied to the motor, which in turn alters the motor's speed and the oscillator's vibration frequency, ranging from 5.0 Hz to 40.0 Hz, depending on the required cyclic frequency for testing. The machine that produces the harmonic vibrations is shown in Fig. 4.

Soil mechanics relies heavily on stress sensors, which measure total soil pressure, typically with a capacity of 100 kPa. Soil properties, including strength, compressibility, and stability, can be evaluated with their help [19]. The shape of the stress sensor is illustrated in Fig. 5.

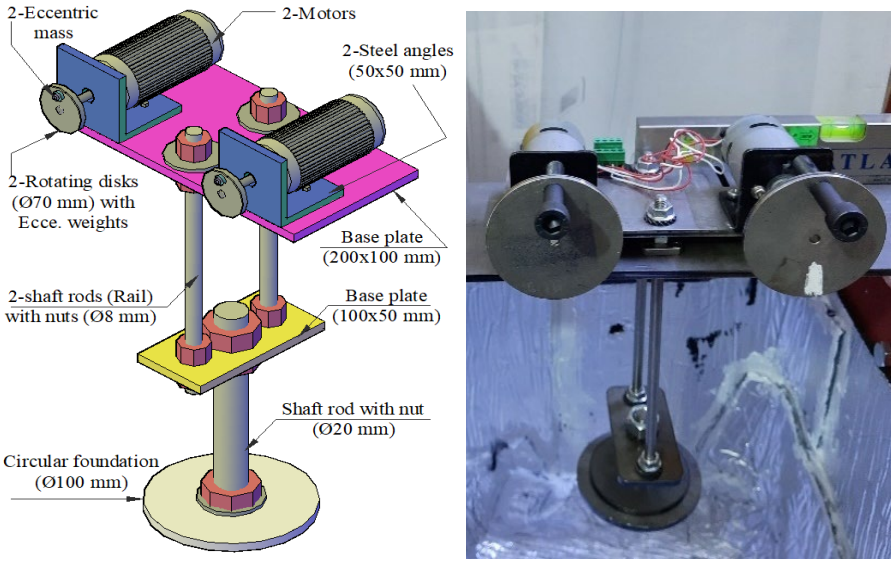

Figure 4. Harmonic vibration generator (mechanical oscillator).

The accelerometer sensor records acceleration along three axes (X, Y, and Z) with adjustable ranges and resolutions, capturing both dynamic accelerations induced by motion or impact, as well as static acceleration due to gravity. The sensor has a measurement capacity of up to 16 g. Data collected by the accelerometer and its recorder were processed using SeismoSignal software to compute displacement, velocity, and acceleration time histories for each axis and at sensor locations within or around the soil model. The accelerometer is illustrated in Fig. 6.

Figure 5. Stress sensors.

Figure 6. Accelerometer sensor.

Measuring pore water pressure is crucial for assessing soil behavior. In this study, a suction pressure sensor with a range of −100 kPa to +100 kPa was used to monitor the pressure difference (i.e., Ua-Uw) between pore air and pore water. Negative values indicate suction (tensile state), while positive values show compression.

The Linear Variable Differential Transformer (LVDT) is an electromechanical transducer that converts linear mechanical displacement into a proportional electrical signal. LVDTs are widely used as

displacement meters due to their high precision, which enables them to measure movements as small as a few micrometers.

Soil moisture, pH, and light intensity were measured using portable soil meters. Two different devices were employed to assess moisture conditions in both unsaturated and saturated soil specimens. The models of the meters and their specifications are presented in Fig. 7.

a. Model of (SKU-6281) **b. Model of (BAF-2.0)**

Figure 7. The soil moisture meters.

2.4. Preparation of the Model for the Test

The subsequent assessment method may be demonstrated*:*

1. To ensure uniform density, the soil sample was placed in successive layers. The net surface area of the model box was approximately 480 × 480 mm, with each layer compacted to a thickness of 50 mm.
2. The gypseous soil was first weighed to determine its target density (loose or medium). It was then placed in the box and compacted manually using a steel or wooden tamper until a uniform 50 mm layer was achieved (Fig. 8a).
3. Figs. 8b and 8c demonstrate the ideal locations for stress and accelerometer sensors inside the model; thus, it is important to follow the instructions in paragraph (2) above until the desired model height (about 500 mm) is obtained.
4. A bubble level was used to make sure the surface was even after the earth was compacted and placed in the steel box.
5. As shown in Fig. 8e, the foundation model, including the harmonic vibration system, was positioned at the plan center (X-Y center) of the box.
6. A single LVDT-equipped magnetic holder was fastened to the sides of the container. The zero reading was obtained by touching the LVDT to the wings at the footing's specified center.
7. Fig. 8e depicts how the models were saturated with water to the desired level: a 50-liter water tank was placed on a wooden table at a height of 500 mm, and a plastic tube with a diameter of 6 mm was connected from the tank to the steel box via the valve at the box's base. After filling the model to capacity with water, the air was forced out of the soil by leaving it uncovered for one day under a double nylon cover, resulting in a fully saturated sample of granular gypseous soil.
8. A piece of plastic pipe (as a cover) with an inner diameter of 102 mm was placed on the soil's surface and around the foundation in order to prevent collapse while preparing a sample with a foundation depth of 0.5 B and 1.0 B. The soil was then sprinkled with a little water using a small water sprinkler until the gypseous soil granules adhered to a small degree and protected it from collapsing. As shown in Fig. 8f, the ring was cut transversely to allow for easy insertion and removal of the pipe section from the foundation system. Additionally, the granular soil sample had already absorbed the necessary amount of water before the test commenced.
9. A harmonic vibration system was used to apply dynamic loads. Fig. 8g displays tension, pressure, accelerometer, and LVDT sensor data over time.

As shown in Fig. 8h, the cyclic frequencies are maintained until failure occurs or the target strain ratio is reached.

The case numbers, model configurations, and experimental variables are summarized in Table 3. The main parameters considered were:

- Saturation degree: three levels were tested (6 %, 60 %, and 100 %);
- Depth of foundation: foundations were embedded at 0.5 B and 1.0 B below the soil surface to assess the effect of embedment on dynamic response;
- Depth of sensors: stress and accelerometer sensors were installed at 0.5 B and 1.0 B to evaluate vibration penetration with depth;
- Eccentric mass: two eccentric masses (28 g and 44.8 g) were applied using the harmonic vibration machine, corresponding to operating frequencies of 9 Hz, 12 Hz, and 15 Hz.

a. Compaction of soil at 5 cm layer

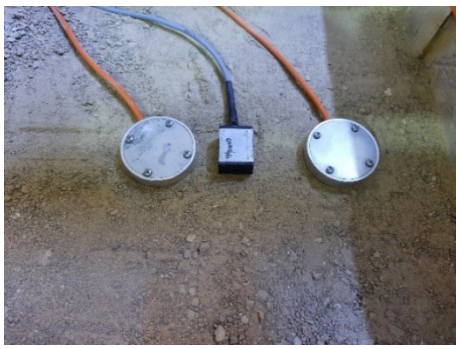

b. Placing sensors inside a model

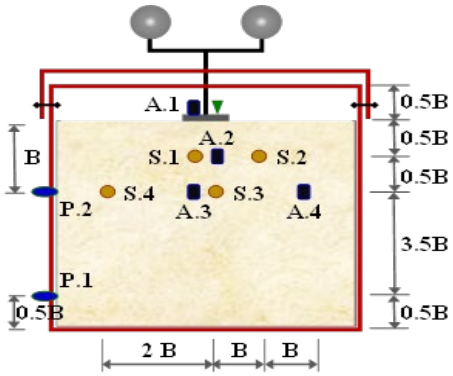

c. The distribution of sensors

d. Placing of foundation at a center

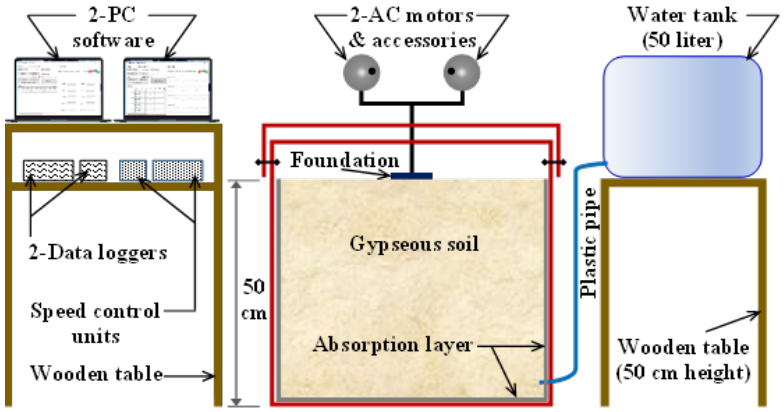

e. The harmonic vibration and soil in the model box with equipment

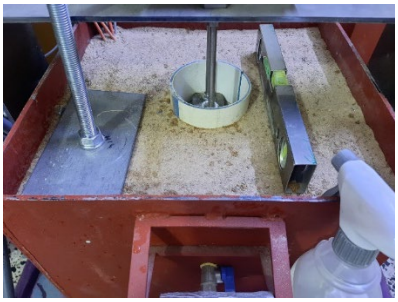


f. Preparing a model at depth foundation (D_f = 0.5 B or 1.0 B)


g. Beginning of the test **h. The model at failure state**

Figure 8. A summary of model preparatory procedures up until their failure.

Table 3. Case studies and models with explanatory variables.

Model details and variable factors			At D_f (0.0B)		At D_f (0.5B)		At D_f (1.0B)	
S_r (%)	m_e (gm)	f_n (Hz)	D_f (mm)	Case No.	D_f (mm)	Case No.	D_f (mm)	Case No.
		9		1		19		37
	28.0	12		2		20		38
Dry (Natural)		15		3		21		39
6%		9		4		22		40
	44.8	12		5		23		41
		15		6		24		42
		9		7		25		43
	28.0	12	0.0 B	8	0.5 B	26	1.0 B	44
Unsaturated		15		9		27		45
60%		9	(0.0)	10	(50.0)	28	(100)	46
	44.8	12	mm	11	mm	29	mm	47
		15		12		30		48
		9		13		31		49
	28.0	12		14		32		50
Saturated		15		15		33		51
100%		9		16		34		52
	44.8	12		17		35		53
		15		18		36		54

Three frequencies 9 Hz, 12 Hz, and 15 Hz were used in this study to calculate D_z, B_z, A_z, k_z, ω_n, c_z, f_n, f_m, m, and G for each frequency, as shown in Equations (1) to (12) [20].

$$D_z = \frac{c_z}{c_{cz}} = \frac{0.425}{\sqrt{B_z}}; \quad (1)$$

$$B_z = \left[\left(\frac{1-\mu}{4}\right)\times\left(\frac{m}{\rho r_o^3}\right)\right] = \left[\left(\frac{1-\mu}{4}\right)\times\left(\frac{W}{\gamma r_o^3}\right)\right]; \quad (2)$$

$$m = \frac{W}{g}; \quad (3)$$

$$c_z = \frac{(3.4r_o)}{(1-\mu)}\sqrt{G\rho}; \quad (4)$$

$$c_{cz} = 2\omega_n m = 2\sqrt{k_z m}; \quad (5)$$

$$G = \frac{k_z(1-\mu)}{4r_o}; \quad (6)$$

$$k_z = \left(\frac{4Gr_o}{1-\mu}\right) = \left[m(2\pi f_n)^2\right] = m\omega^2 = \frac{P}{u}; \quad (7)$$

$$\omega = \omega_n = 2\pi f_n = \sqrt{k_{z/m}} = \sqrt{g/u}; \quad (8)$$

$$f_n = \frac{1}{2\pi}\sqrt{\frac{k_z}{m}}; \quad (9)$$

$$f_m = \frac{f_n}{\sqrt{\left(1-2D_z^2\right)}}; \quad (10)$$

$$A_z = \left(\frac{2m_e e_o}{m}\right)\times\left(\frac{B_z}{0.85\sqrt{B_z - 0.18}}\right); \quad (11)$$

$$Q(t) = m\ddot{u} + c_z\dot{u} + k_z u, \quad (12)$$

where, D_z = Damping ratio; B_z = Modified mass ratio; c_z = Coefficient of damping; c_{cz} = Coefficient of critical damping in (N-sec/m); m, W = Total machinery and foundation masses in (kg) and (kN), respectively; ρ, γ = Soil density in (kg/m^3) and (kN/m^3), respectively; g = Ground acceleration (g = 9.81 m/sec^2); μ = Poisson's ratio; r_o = Radius of the circular foundation (radius of the loaded area) in (m); G = Dynamic shear modulus of the soil in (kPa); k_z = Static Spring constant (N/m); ω_n = Rotating masses' natural circular frequency in (rad/sec); f_n = Frequency of natural circular in (Hz); f_m = Resonant frequency in (Hz); A_z = Amplitude of the vibration at frequency resonance in (mm); mRe = The mass of eccentricity in (kg); $eROR$ = The distance of eccentricity in (mm); P = The maximum of vertical load (N); $Q(t)$ = Total force in (N); u = Displacement in (mm); $\dot{u}$ = Velocity in (m/sec); and $\ddot{u}$ = Acceleration in (m/sec^2).

3. Results and Discussion

Fig. 9 presents representative time histories of settlement, acceleration, velocity, displacement, total stresses, and suction pressure obtained from the model tests. For clarity, one case model was selected for each saturation condition (natural, partially saturated, and fully saturated) to illustrate the general response, since the overall shapes of the dynamic curves were similar, differing mainly in average magnitudes. Figs. 10–21 further illustrate the relationships between dynamic soil properties and operating frequency (f_n) or degree of saturation (S_r), considering additional variables such as foundation depth (D_f) and eccentric mass (m_e).

In general, Figs. 10, 12, 14, 16, 18, and 20 illustrate the variation of gypseous soil dynamic properties with operating frequency at different foundation depths (0.0 B, 0.5 B, and 1.0 B) and eccentric masses (28 g and 44.8 g). In contrast, Figs. 11, 13, 15, 17, 19, and 21 illustrate the impact of saturation degree on the same dynamic properties under identical foundation depths and eccentric masses.

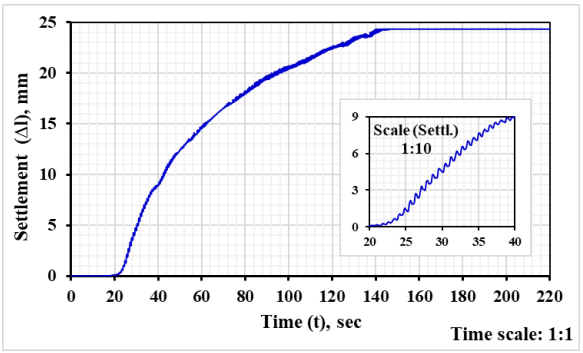

a. Settlement–Time curve

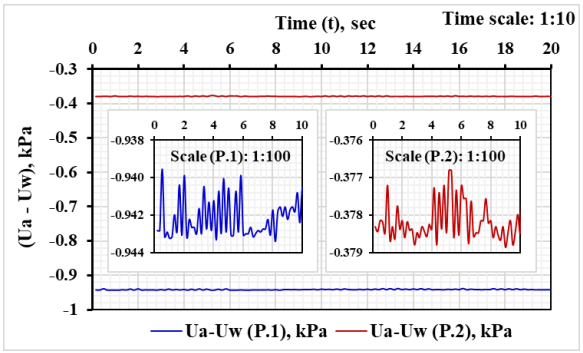

b. Suction pressure–Time curves

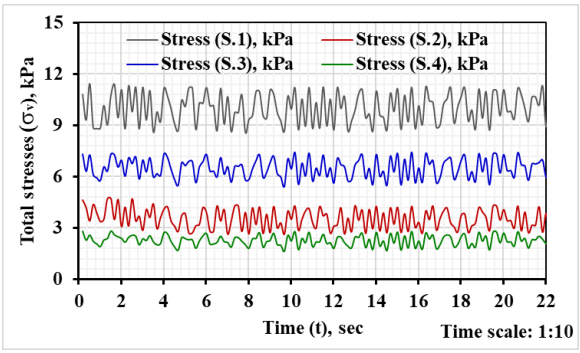

c. Total stress–Time curves at points number 1 to 4

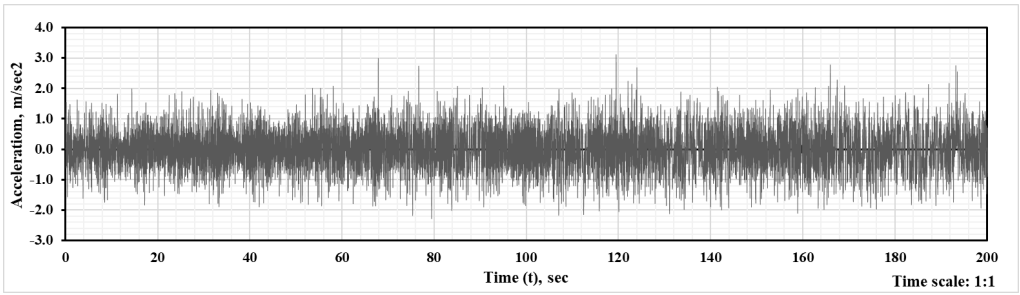

d1. Acceleration–Time curve at point number 1

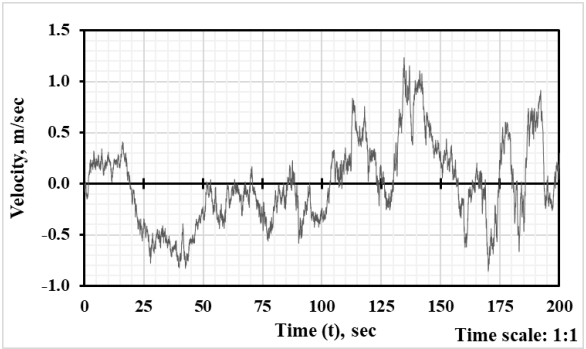

d2. Velocity–Time curve at point 1

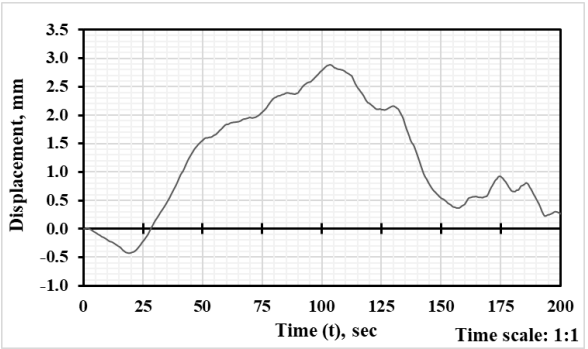

d3. Displacement–Time curve at point 1

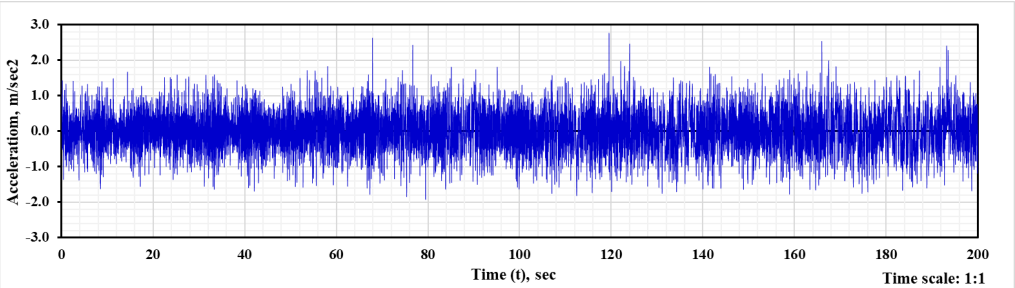

e1. Acceleration–Time curve at point number 2

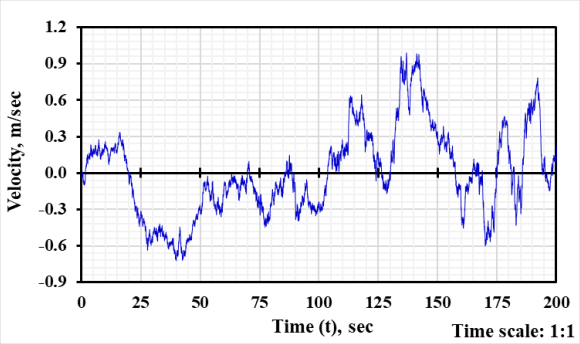

e2. Velocity–Time curve at point 2

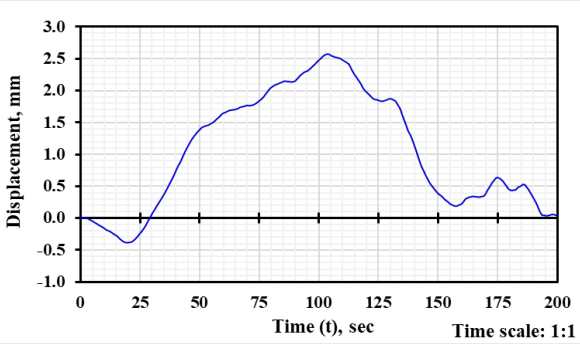

e3. Displacement–Time curve at point 2

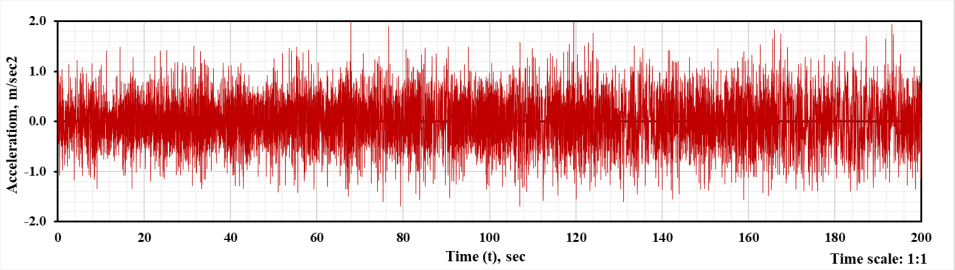

f1. Acceleration–Time curve at point number 3

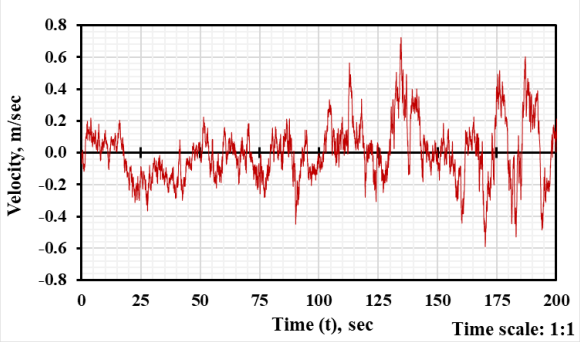

f2. Velocity–Time curve at point 3

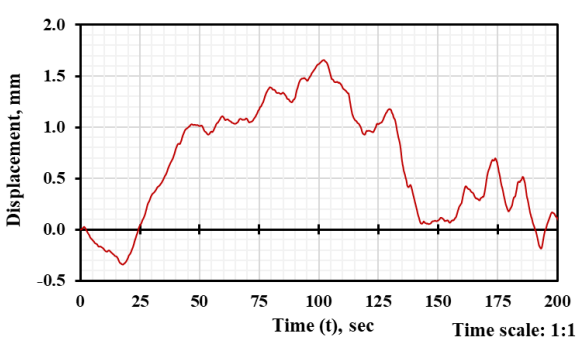

f3. Displacement–Time curve at point 3

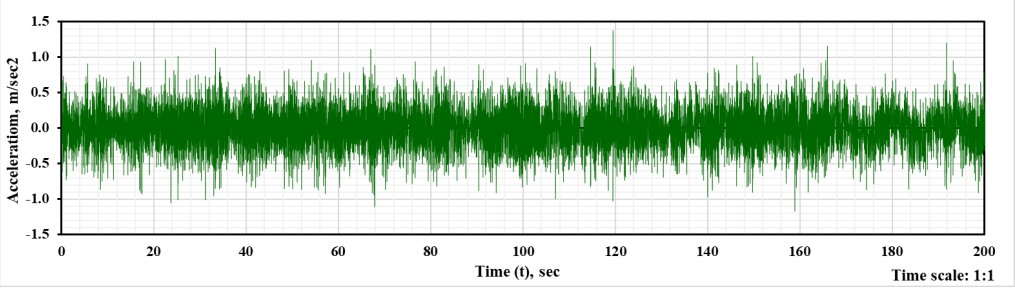

g1. Acceleration–Time curve at point number 4

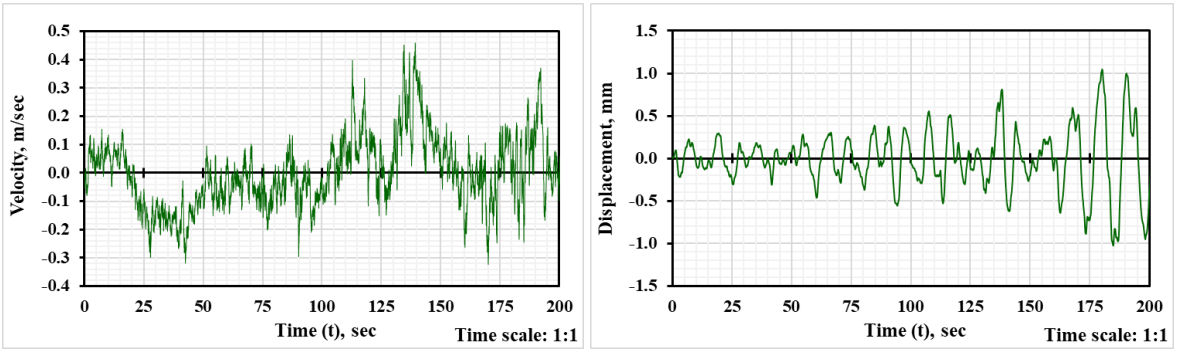

g2. Velocity–Time curve at point 4 g3. Displacement–Time curve at point 4

Figure 9. Typical dynamic characteristics at 100 percent saturation.

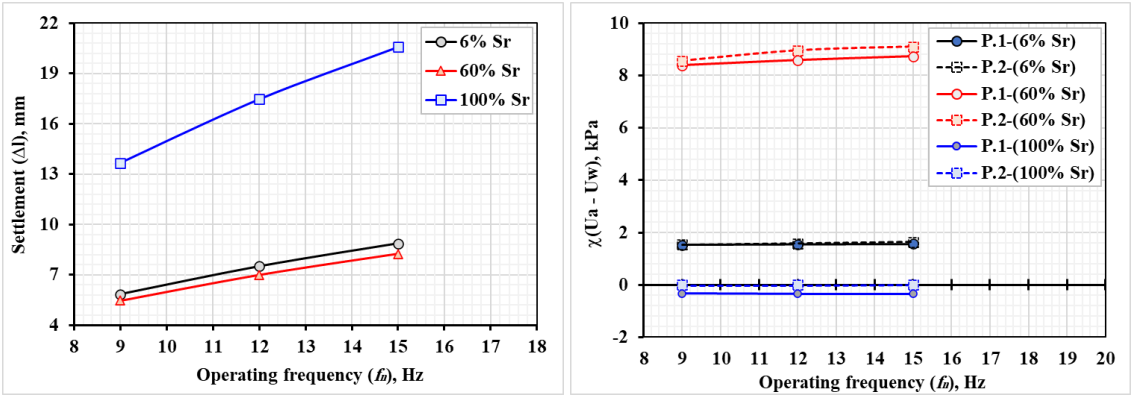

a. Settlement–Frequency curves b. Suction stress–Frequency curves

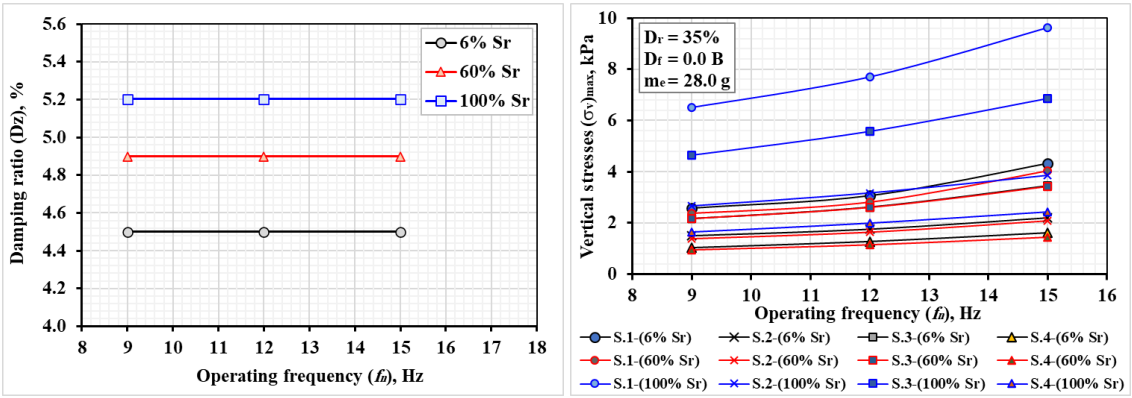

c. Damping ratio–Frequency curves d. Vertical stresses–Frequency curves

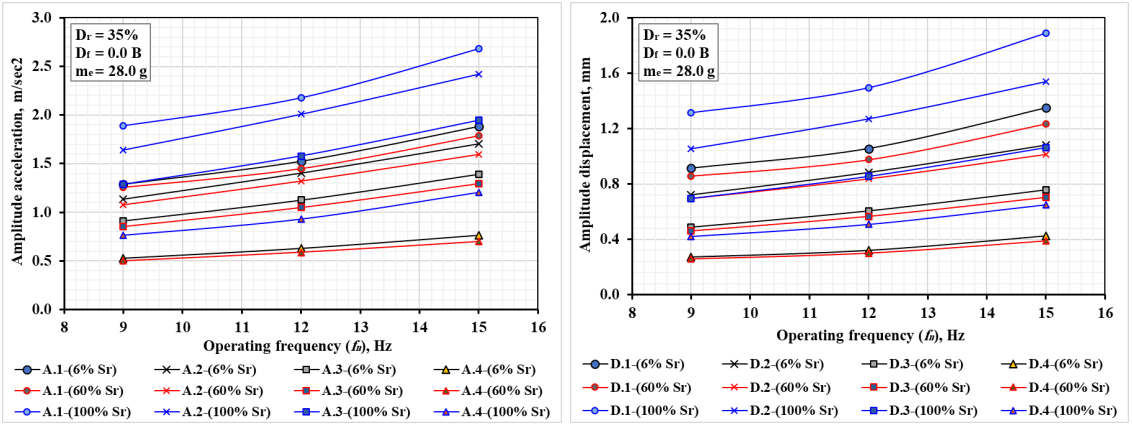

e. Acceleration–Frequency curves f. Displacement–Frequency curves

Figure 10. The behavior of gypseous soil's dynamic properties at different operating frequencies for case study numbers 1, 2, 3, 7, 8, 9, 13, 14, and 15, with m_e = 28.0 g, D_f = 0.0 B, and D_r = 35%.

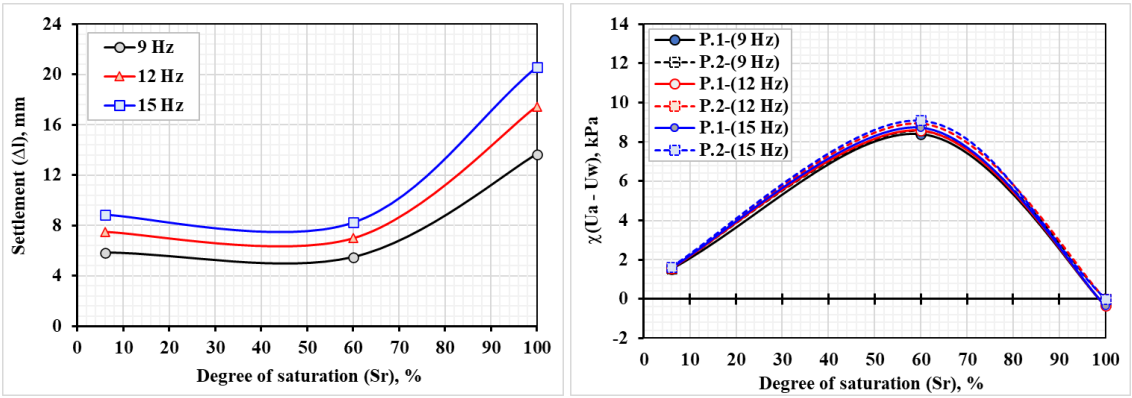

a. Settlement–Saturation degree curves

b. Suction stress–Sr curves

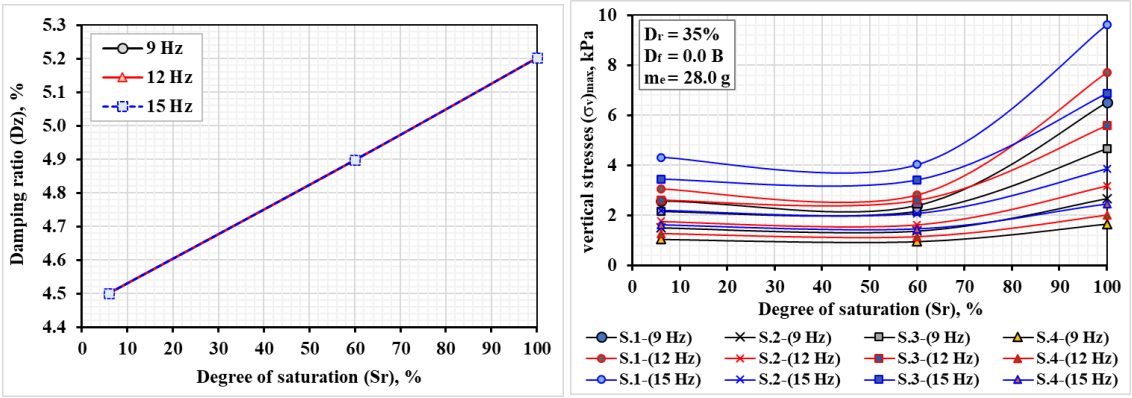

c. Damping ratio–Sr curves

d. Vertical stresses–Sr curves

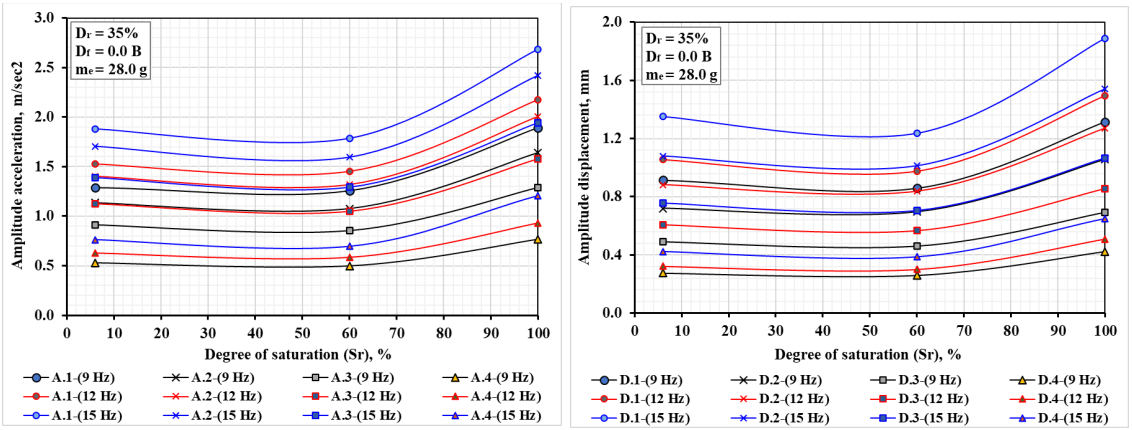

e. Acceleration–Sr curves

f. Displacement–Sr curves

Figure 11. The behavior of gypseous soil's dynamic properties at different saturation levels with m_e = 28.0 g, D_f = 0.0 B, and D_r = 35% for case study numbers 1, 2, 3, 7, 8, 9, 13, 14, and 15.

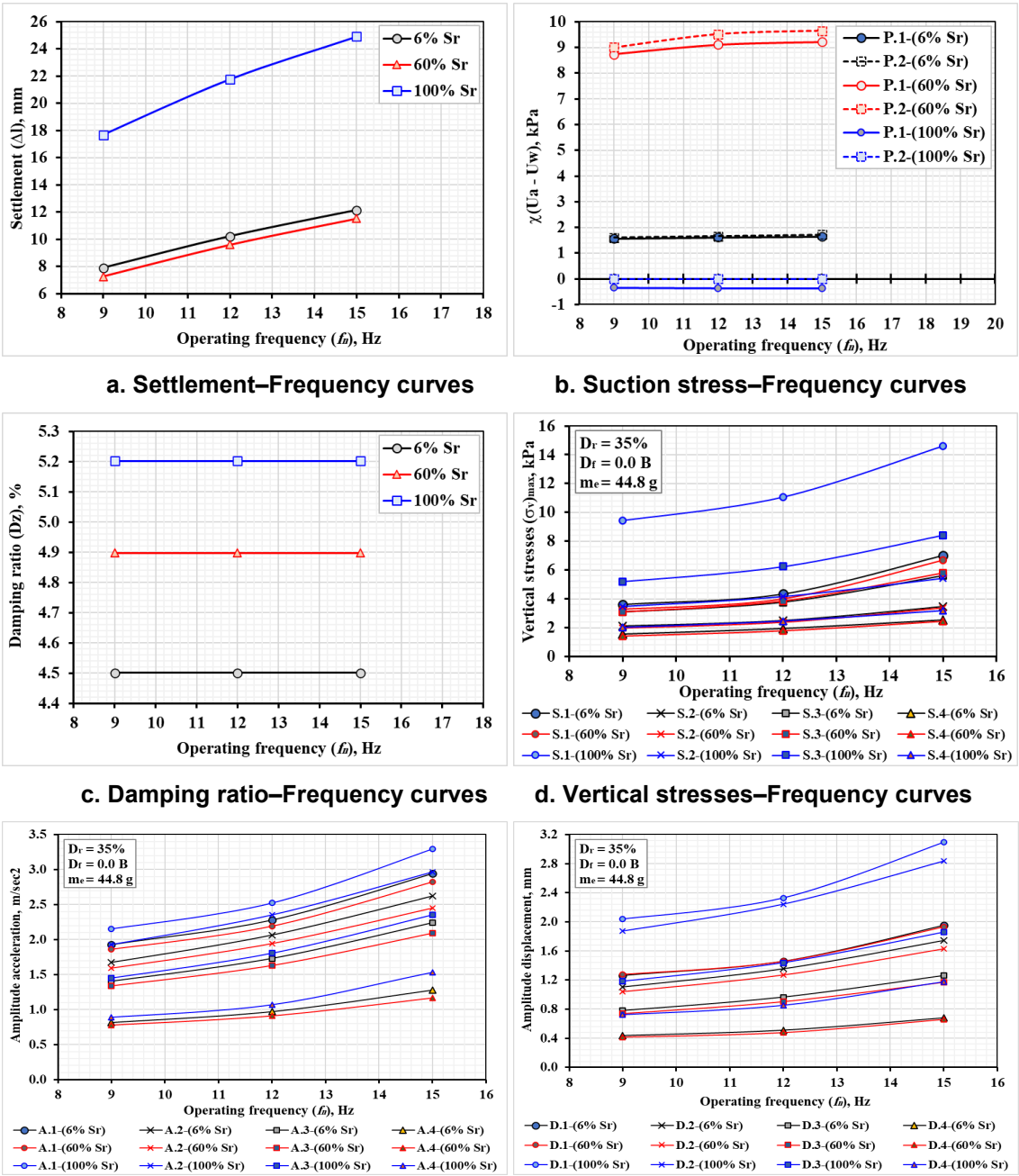

a. Settlement–Frequency curves **b. Suction stress–Frequency curves**

c. Damping ratio–Frequency curves **d. Vertical stresses–Frequency curves**

e. Acceleration–Frequency curves **f. Displacement–Frequency curves**

Figure 12. The behavior of gypseous soil's dynamic properties with varying operating frequencies at m_e = 44.8 g, D_f = 0.0 B, and D_r = 35% for case study numbers 4, 5, 6, 10, 11, 12, 16, 17, and 18.

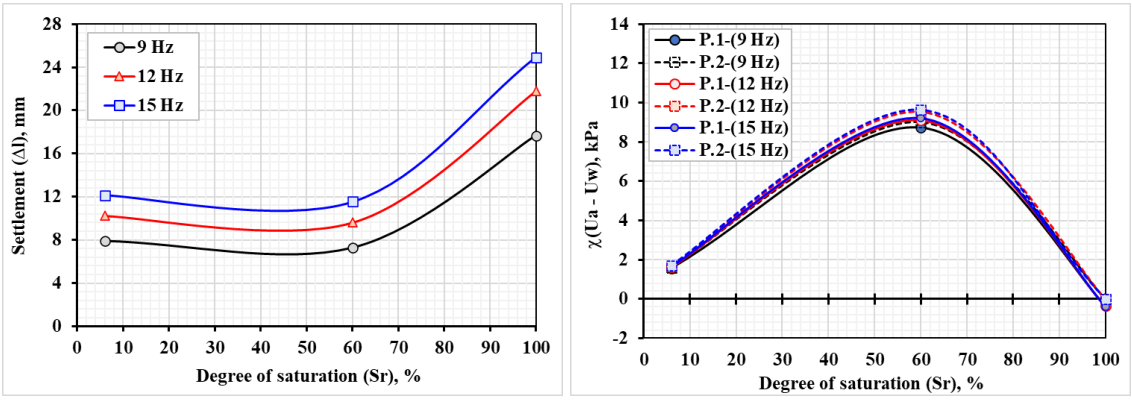

a. Settlement–Saturation degree curves

b. Suction stress–Sr curves

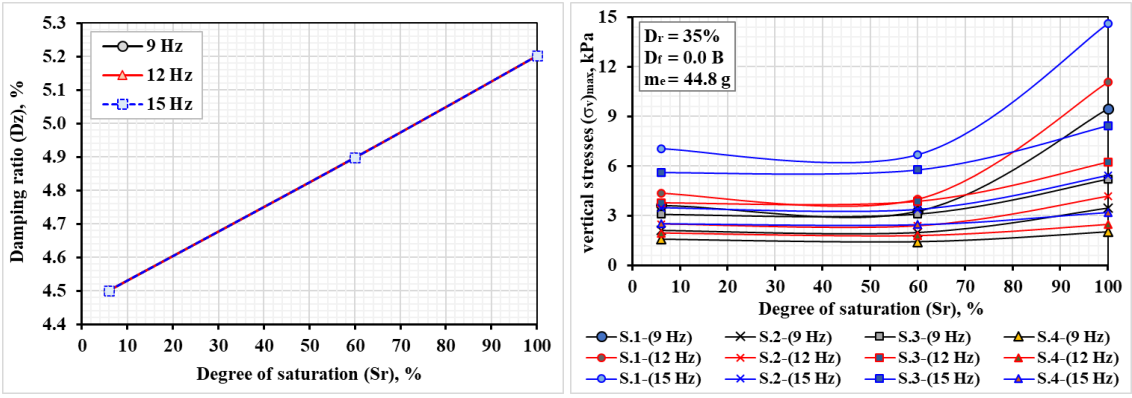

c. Damping ratio–Sr curves

d. Vertical stresses–Sr curves

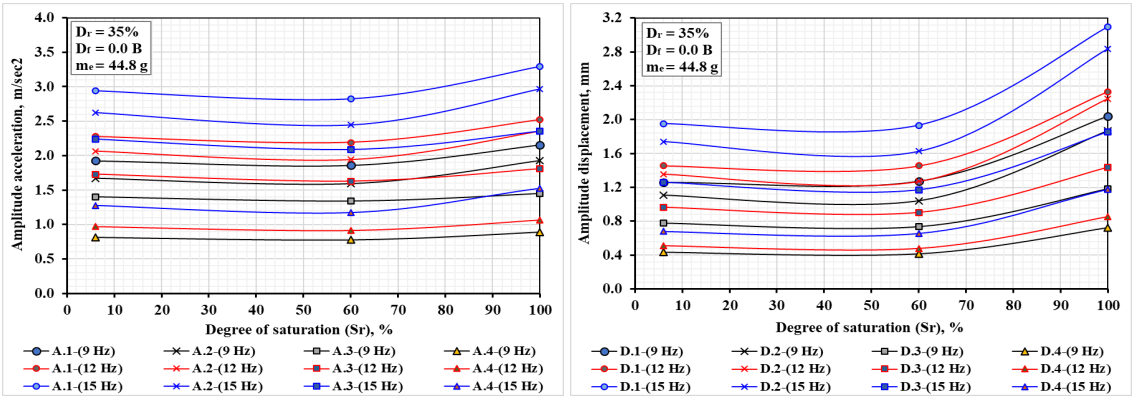

e. Acceleration–Sr curves

f. Displacement–Sr curves

Figure 13. The behavior of gypseous soil's dynamic properties with varying degrees of saturation for case study numbers 4, 5, 6, 10, 11, 12, 16, 17, and 18 at m_e = 44.8 g, D_f = 0.0 B, and D_r = 35%.

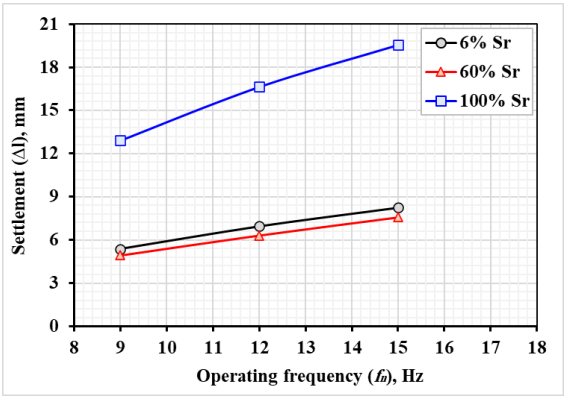

a. Settlement–Frequency curves

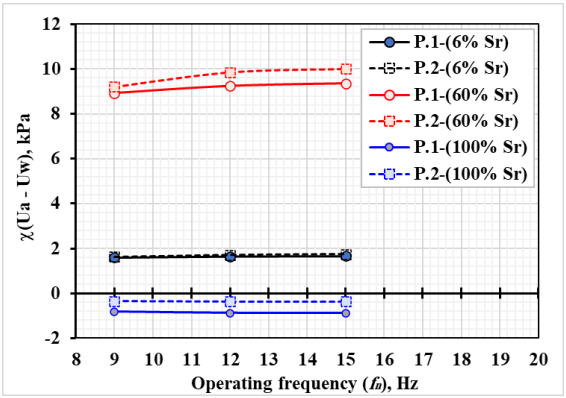

b. Suction stress–Frequency curves

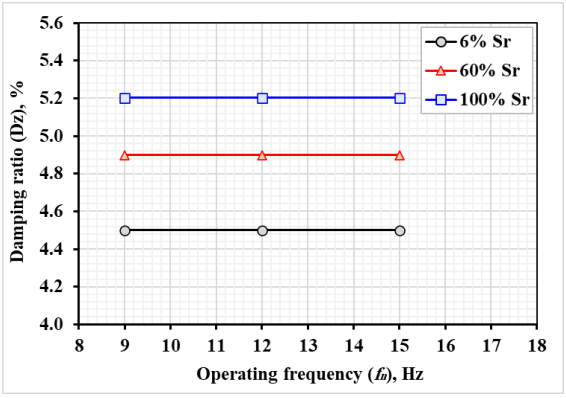

c. Damping ratio–Frequency curves

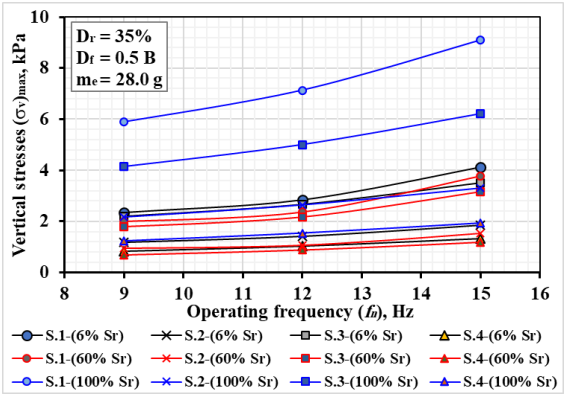

d. Vertical stresses–Frequency curves

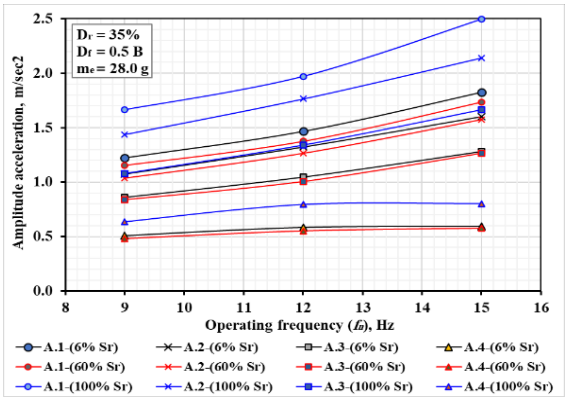

e. Acceleration–Frequency curves

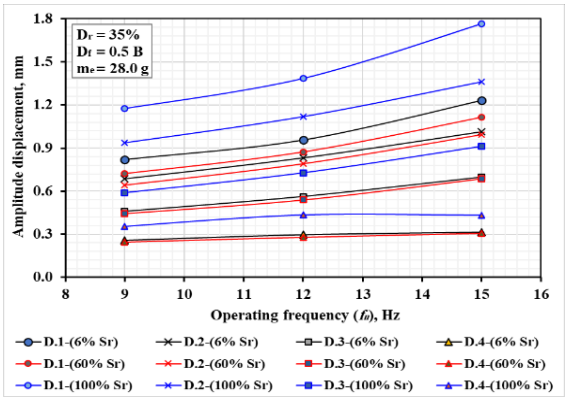

f. Displacement–Frequency curves

Figure 14. The behavior of gypseous soil's dynamic properties at various operating frequencies with m_e = 28.0 g, D_f = 0.5 B, and D_r = 35% for case studies numbered 19, 20, 21, 25, 26, 27, 31, 32, and 33.

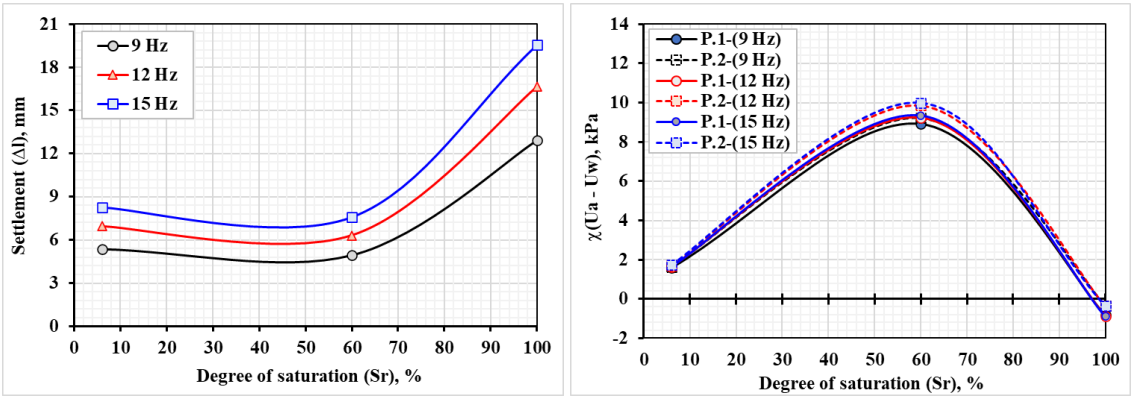

a. Settlement–Saturation degree curves

b. Suction stress–Sr curves

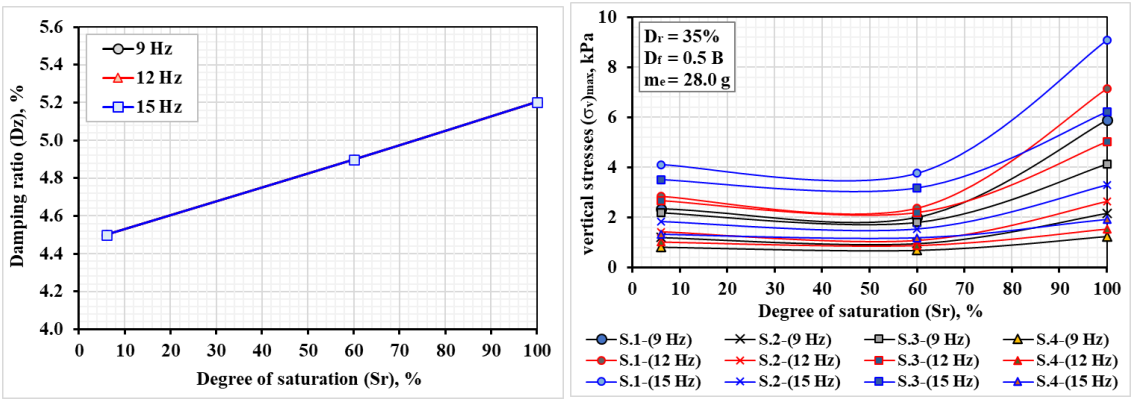

c. Damping ratio–Sr curves

d. Vertical stresses–Sr curves

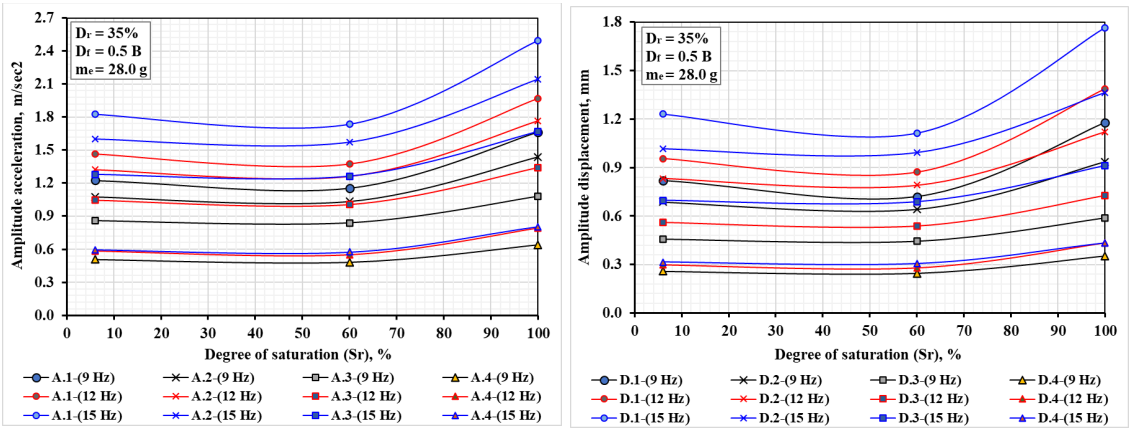

e. Acceleration–Sr curves

f. Displacement–Sr curves

Figure 15. The behavior of gypseous soil's dynamic properties with varying degrees of saturation at m_e = 28.0 g, D_f = 0.5 B, and D_r = 35% for case study numbers 19, 20, 21, 25, 26, 27, 31, 32, and 33.

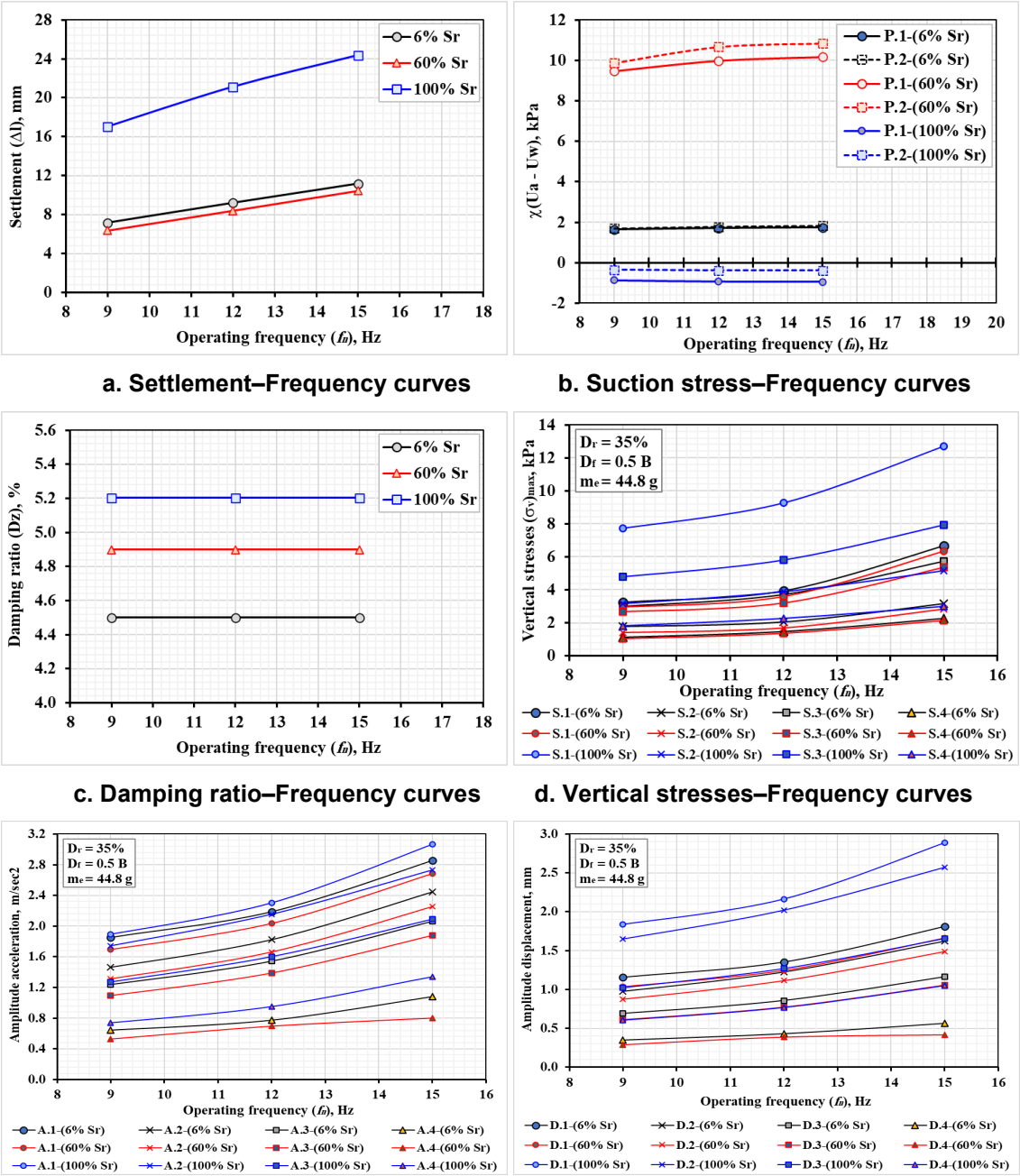

a. Settlement–Frequency curves **b. Suction stress–Frequency curves**

c. Damping ratio–Frequency curves **d. Vertical stresses–Frequency curves**

e. Acceleration–Frequency curves **f. Displacement–Frequency curves**

Figure 16. The behavior of gypseous soil's dynamic properties under varying operating frequencies at m_e = 44.8 g, D_f = 0.5 B, and D_r = 35% for case study numbers 22, 23, 24, 28, 29, 30, 34, 35, and 36.

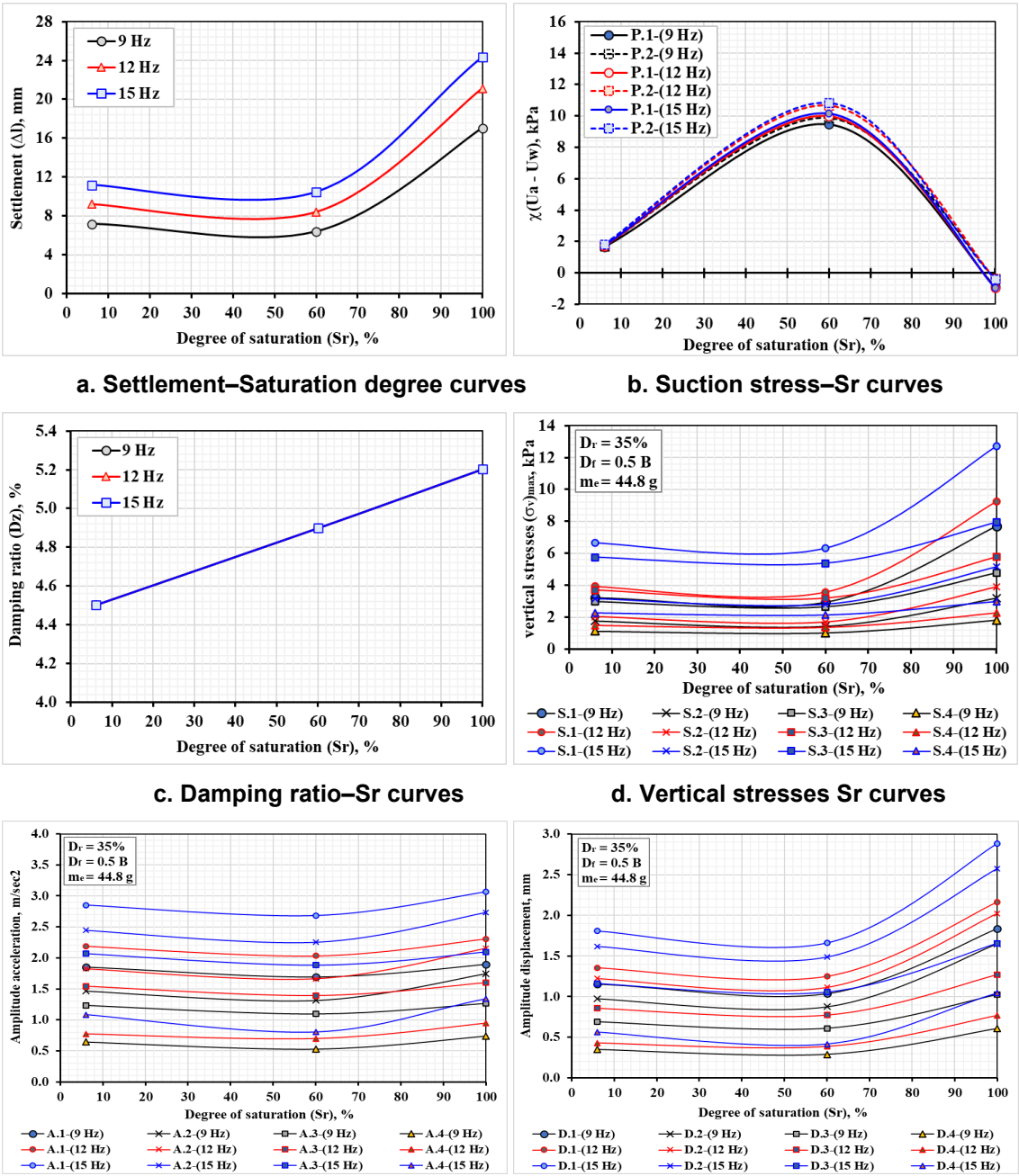

a. Settlement–Saturation degree curves **b. Suction stress–Sr curves**

c. Damping ratio–Sr curves **d. Vertical stresses Sr curves**

e. Acceleration–Sr curves **f. Displacement–Sr curves**

Figure 17. The behavior of gypseous soil's dynamic properties with varying degrees of saturation at m_e = 44.8 g, D_f = 0.5 B, and D_r = 35% for case study numbers 22, 23, 24, 28, 29, 30, 34, 35, and 36.

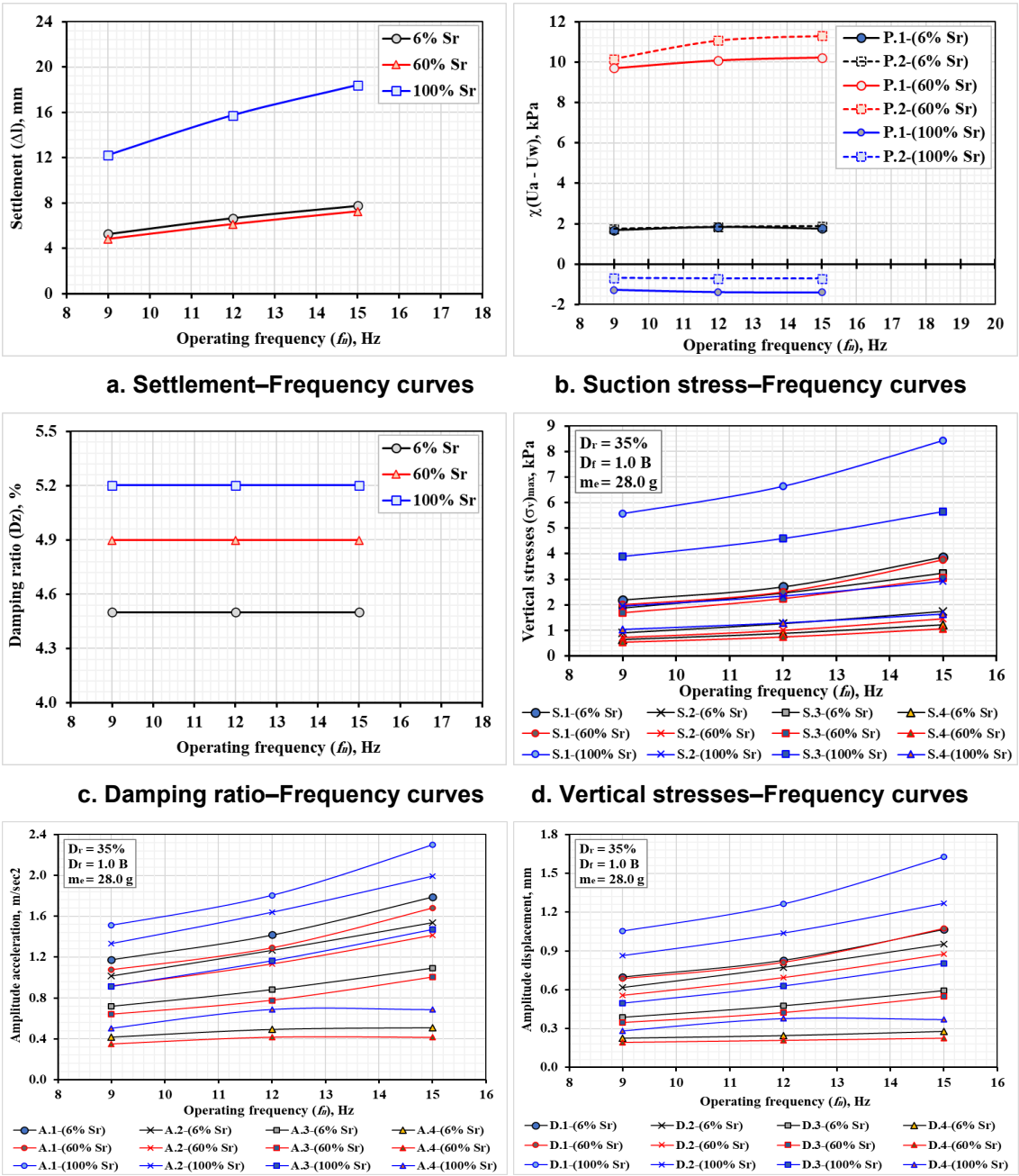

a. Settlement–Frequency curves **b. Suction stress–Frequency curves**

c. Damping ratio–Frequency curves **d. Vertical stresses–Frequency curves**

e. Acceleration–Frequency curves **f. Displacement–Frequency curves**

Figure 18. The dynamic properties of gypseous soil behavior with varying operating frequencies at m_e = 28.0 g, D_f = 1.0 B, and D_r = 35% for case study numbers 37, 38, 39, 43, 44, 45, 49, 50, and 51.

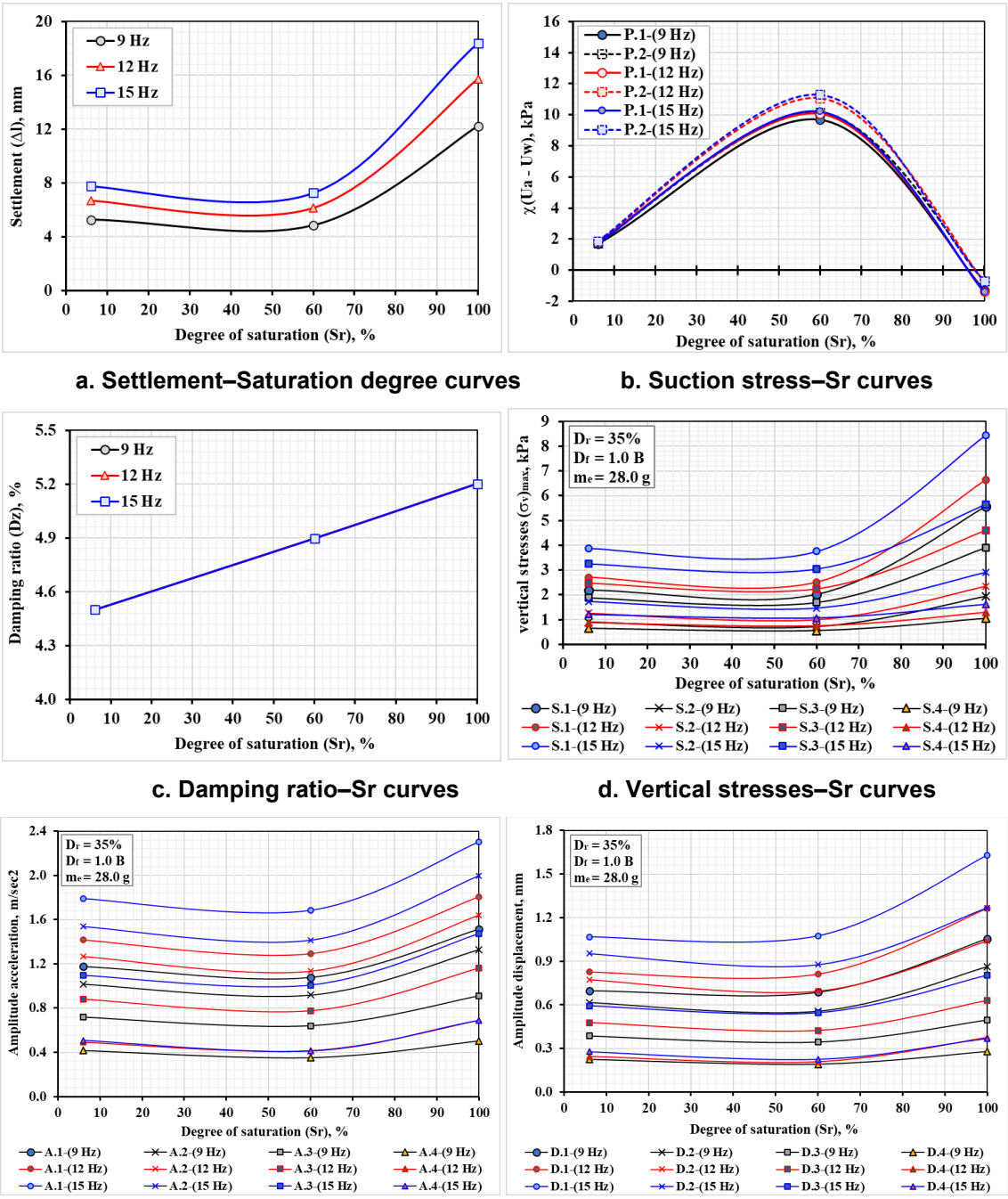

a. Settlement–Saturation degree curves

b. Suction stress–Sr curves

c. Damping ratio–Sr curves

d. Vertical stresses–Sr curves

e. Acceleration–Sr curves

f. Displacement–Sr curves

Figure 19. The behavior of gypseous soil's dynamic properties with varying degrees of saturation at m_e = 28.0 g, D_f = 1.0 B, and D_r = 35% for case study numbers 37, 38, 39, 43, 44, 45, 49, 50, and 51.

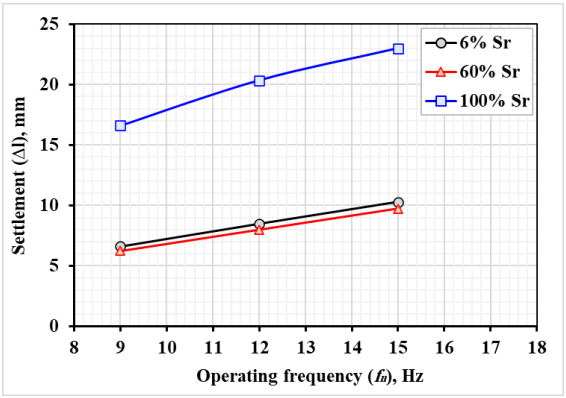

a. Settlement–Frequency curves

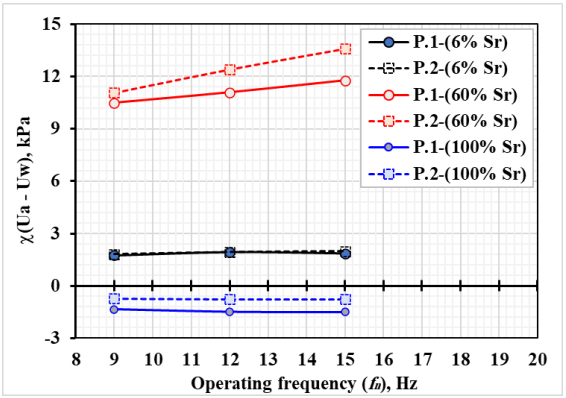

b. Suction stress–Frequency curves

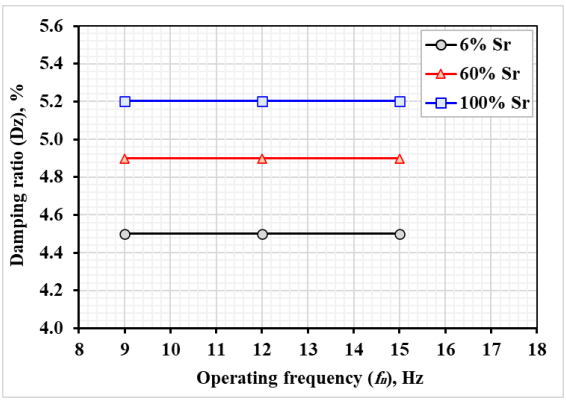

c. Damping ratio–Frequency curves

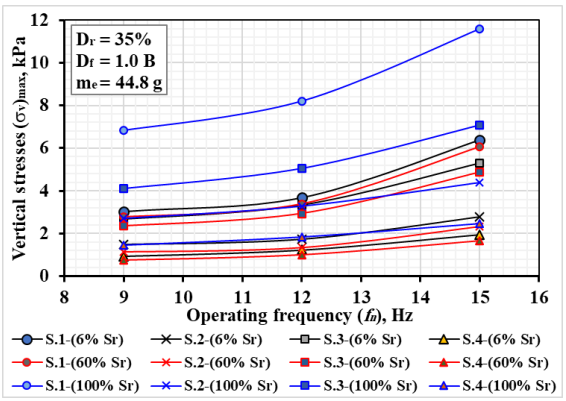

d. Vertical stresses–Frequency curves

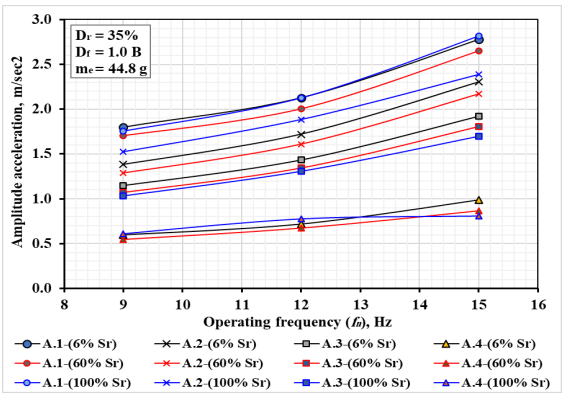

e. Acceleration–Frequency curves

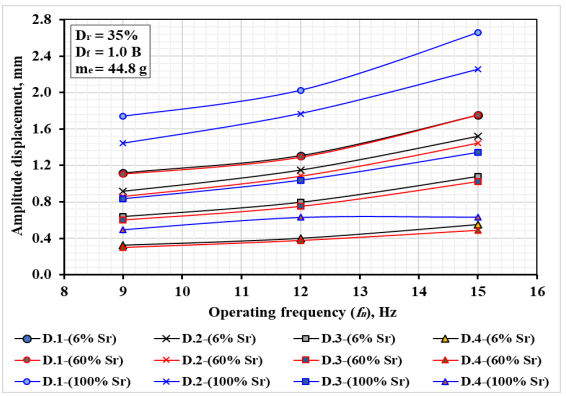

f. Displacement–Frequency curves

Figure 20. The behavior of gypseous soil under dynamic properties with varying operating frequencies at m_e = 44.8 g, D_f = 1.0 B, and D_r = 35% for case study numbers 40, 41, 42, 46, 47, 48, 52, 53, and 54.

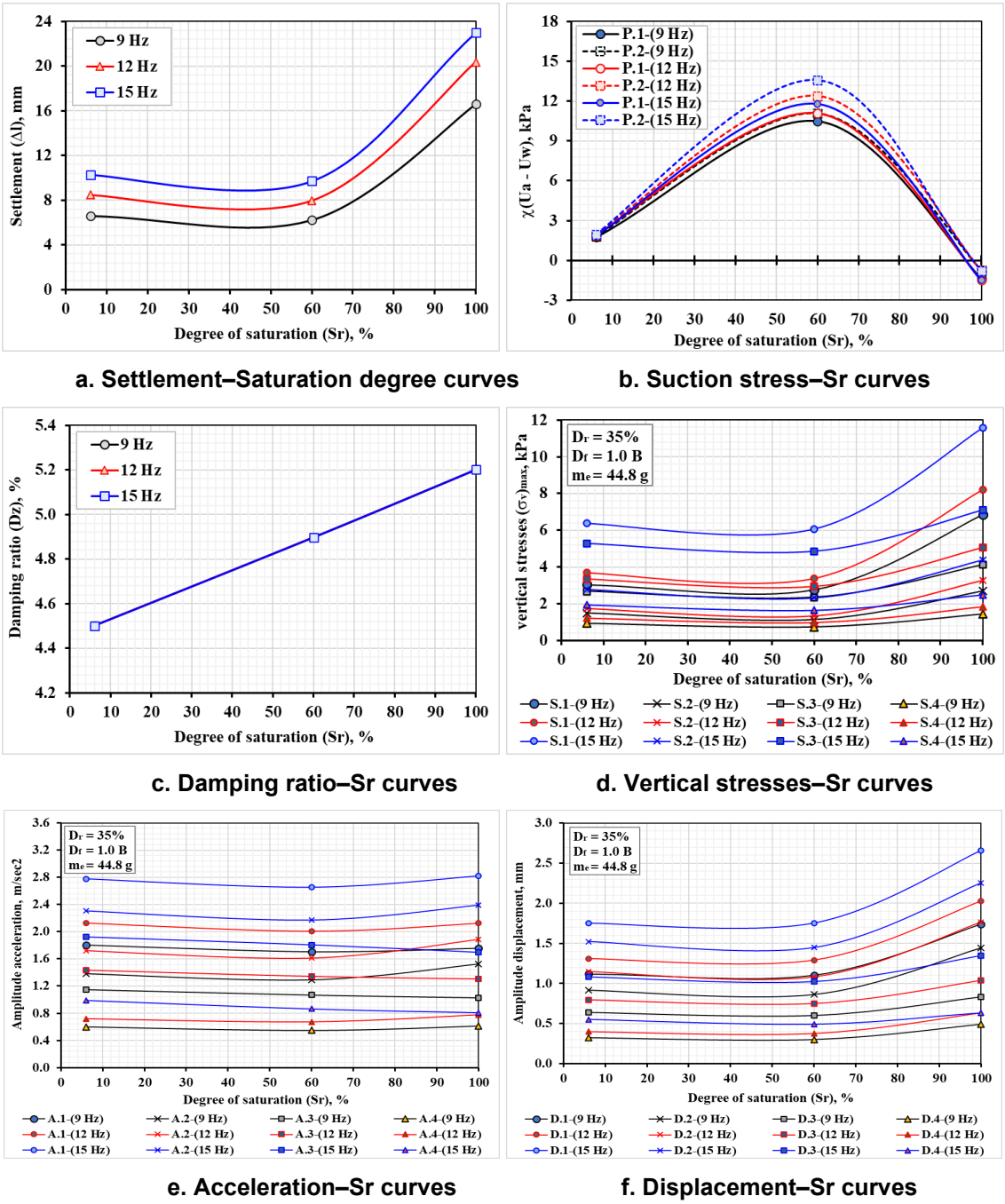

a. Settlement–Saturation degree curves **b. Suction stress–Sr curves**

c. Damping ratio–Sr curves **d. Vertical stresses–Sr curves**

e. Acceleration–Sr curves **f. Displacement–Sr curves**

Figure 21. The behavior of gypseous soil's dynamic properties with varying degrees of saturation for case studies 40, 41, 42, 46, 47, 48, 52, 53, and 54, with m_e = 44.8 g, D_f = 1.0 B, and D_r = 35%.

As shown in Fig. 1, sand is the predominant fraction of the tested soil, with 79 % sand and 1 % gravel, while 20 % passed the No. 200 sieve. Based on the classification results, the gypseous soil from Tikrit is identified as "SM" (silty sand) according to the Unified Soil Classification System (USCS).

The results showed that the tested soil contained 45.0 % gypsum ($CaSO_4$), which is consistent with the findings reported by the authors [21] and [22]. The carbonate content ($CaCO_3$) was relatively high, which typically imparts greater shear strength to soils in their natural or slightly unsaturated state due to the limited presence of clay minerals. The total sulfate content (SO_3) was also elevated, indicating potential interaction with reinforced concrete foundations under wet conditions. The measured pH value of 7.23 reflects a neutral chemical environment. The organic matter content was very low (0.72 %), which explains the pale color and lack of odor in the soil. Additionally, the high level of total soluble salts (TSS) suggests influence from a shallow groundwater table during winter or following irrigation.

The authors [23] conducted preliminary research on the chemical properties of water and their influence on soil behavior. The study demonstrated that water chemistry has a significant impact on the rate and extent of gypseous soil disintegration. Distilled water was found to be more aggressive than saline

water, accelerating the dissolution of gypsum. During the early stages of hydration, gypsum is primarily produced through modifications in the formation of calcium silicate hydrate, making it a key binding agent that contributes to soil stability. In gypseous soils, sulfate ions released from gypsum interact with the alumina phase. When gypsum remains dry, the mechanical response of gypseous soils is similar to that of non-gypsum soils under loading. However, sudden exposure to large volumes of pure water destroys the chemical bonds between gypsum and soil particles, leading to rapid collapse and loss of strength.

Accurate evaluation of ground response in soil–structure interaction, particularly under cyclic and dynamic loading, requires reliable models for shear modulus and damping ratio across a wide range of strains, as soil energy dissipation must be adequately represented. Building on earlier formulations for the initial shear modulus of unsaturated soils, the authors [7] proposed models that incorporate average skeleton stress, bonding variable, void ratio, and degree of saturation to predict shear modulus, damping ratio, and shear strain behavior.

Experimental results of the present study indicate that, under constant soil saturation, foundation depth, and eccentric mass, the dynamic properties of gypseous soil (settlement, acceleration, velocity, displacement, total stress, and suction pressure) increase progressively with operating frequency (Figs. 10, 12, 14, 16, 18, and 20). This trend is attributed to higher cyclic and dynamic stresses imposed beneath the machine foundation at elevated frequencies. However, due to wave damping within the soil, the magnitude of these responses diminishes with increasing distance from the foundation center in both vertical and horizontal directions.

At constant operating frequency and identical testing conditions (saturation, foundation depth, and eccentric mass), Figs. 11, 13, 15, 17, 19, and 21 demonstrate that the dynamic properties of gypseous soil – settlement, acceleration, velocity, displacement, total stress, and suction pressure – are strongly influenced by the degree of saturation. The soil exhibits maximum stiffness and shear strength at an intermediate saturation of 60%, where matric suction peaks, while strength decreases sharply at full saturation (100 % Sr). The damping ratio, in contrast, increased steadily with saturation, from about 4.5 % at 6 % Sr to 4.9 % at 60 % Sr and 5.2 % at 100 % Sr. Compared to the natural condition (6 % Sr), dynamic responses at 60 % Sr are reduced; however, beyond this level, the dissolution of gypsum in water causes bond degradation, leading to increased collapse potential and a higher dynamic response at full saturation.

The dissolution process of gypsum under wetting, particularly under static and cyclic stresses, plays a critical role in soil instability. This process depends on gypsum content, hydraulic gradient, void ratio, and other factors [24].

Quantitatively, the dynamic characteristics of gypseous soil increased with frequency by approximately 50–52 % (settlement), 3–6 % (suction stress), 47–68 % (total stress), 42–46 % (acceleration), and 44–48 % (vertical displacement). With rising saturation up to 60 %, these properties decreased by 6–7 % (settlement and total stress), 2–5 % (acceleration), and 6–9 % (vertical displacement). Between 60 % and 100 % saturation, however, the values rose sharply, reaching increases of 149–150 % (settlement), 139–173 % (total stress), 50–51 % (acceleration), and 52–54 % (vertical displacement). Suction stress showed the opposite trend: it rose dramatically by 453–457 % as saturation increased from 0 % to 60 % then decreased by nearly 100 % (approaching zero) as saturation increased from 60 % to 100 %, reflecting the near-complete loss of matric suction at full saturation.

4. Conclusions

Based on the experimental results and analyses presented in this study, the following conclusions can be drawn:

1. For constant soil saturation, foundation depth, and eccentric mass, the dynamic properties of gypseous soil (acceleration, velocity, displacement, suction pressure, total stress, and settlement) increased progressively with operating frequency.
2. At constant frequency and boundary conditions, the dynamic responses of gypseous soil increased with rising saturation and reached their maximum at full saturation (100 % Sr), where gypsum dissolution degraded interparticle bonding and increased collapse potential.
3. At 60 % saturation, the dynamic properties decreased relative to the natural condition (6 % Sr) by about 7 % (settlement and total stress), 5 % (acceleration), and 9 % (vertical displacement), reflecting maximum stiffness and matric suction at intermediate saturation.
4. Increasing foundation embedment from 0.0 B to 1.0 B reduced the peak dynamic responses of the gypseous soil by approximately 10 % to 15 % (settlement, vertical stress, acceleration, and displacement) at full saturation, owing to the confinement and added vertical stiffness provided by the surrounding soil (Figs. 10, 14, 18).

5. Increasing the eccentric mass from 28 g to 44.8 g (a factor of about 1.6) amplified all dynamic responses at full saturation: settlement and acceleration rose by roughly 17 % to 22 %, vertical stress by about 50 %, and displacement amplitude by about 68 %, consistent with the rotating-mass force scaling as $me \cdot e \cdot \omega^2$ (Figs. 10 and 12).
6. Quantitatively, with increasing frequency, dynamic responses increased by approximately 50–52 % (settlement), 3–6 % (suction stress), 47–68 % (total stress), 42–46 % (acceleration), and 44–48 % (vertical displacement).

References

1. Fredlund, D.G., Rahardjo, H. Soil Mechanics for Unsaturated Soils. John Wiley & Sons. New York, 1993. DOI: 10.1002/9780470172759
2. Ng, C.W., Menzies, B. Advanced Unsaturated Soil Mechanics and Engineering. Taylor and Francis. New York, 2007. DOI: 10.1201/9781482266122
3. Zhou, Y.G., Chen, Y.M. Influence of Seismic Cyclic Loading History on Small Strain Shear Modulus of Saturated Sands. Soil Dynamics and Earthquake Engineering. 2005. 25(5). Pp. 341–353. DOI: 10.1016/j.soildyn.2005.03.001
4. Zhang, J., Andrus, R.D., Juang, C.H. Normalized Shear Modulus and Material Damping Ratio Relationships. Journal of Geotechnical and Geoenvironmental Engineering. 2005. 131(4). Pp. 453–464. DOI: 10.1061/(ASCE)1090-0241(2005)131:4(453)
5. Okur, D.V., Ansal, A. Stiffness Degradation of Natural Fine-Grained Soils during Cyclic Loading. Soil Dynamics and Earthquake Engineering 2007. 27(9). Pp. 843–854. DOI: 10.1016/j.soildyn.2007.01.005
6. Xenaki, V.C., Athanasopoulos, G.A. Dynamic Properties and Liquefaction Resistance of Two Soil Materials in an Earth Fill Dam-Laboratory Test Results. Soil Dynamics and Earthquake Engineering 2008. 28(8). Pp. 605–620. DOI: 10.1016/j.soildyn.2007.10.001
7. Biglari, M., Ashayeri, I. An Empirical Model for Shear Modulus and Damping Ratio of Unsaturated Soils. Proceedings of the Unsaturated Soils: Theory and Practice 2011. Kasetsart University. Thailand, 2011. Pp. 591–595.
8. Abdulrasool, A.S., Fattah, M.Y., Salim, N.M. Displacements and Stresses Induced by Vibrations of Machine Foundation on Clay Soil of Different Degrees of Saturation. Case Studies in Construction Materials. 2022. 17. Article no. e01327. DOI: 10.1016/j.cscm.2022.e01327
9. Das, B.M., Luo, Z. Principles of Soil Dynamics. 3rd ed. Cengage Learning. USA, 2017. 608 p.
10. Sivakumar, V., Kodikara, J., Ohagan, R., Hughes, D., Cairns, P., Mckinley, J.D. Effects of Confining Pressure and Water Content on Performance of Unsaturated Compacted Clay under Repeated Loading. Geotechnique. 2013. 63(8). Pp. 628–640. DOI: 10.1680/geot.10.P.103
11. Chao, Z. Experimental Study and Constitutive Modeling of Cyclic Behavior at Small Strains of Unsaturated Silt at Various Temperatures. Ph.D. Thesis. University of Science and Technology. Hong Kong, 2014.
12. Yuan, B., Huang, X., Li, R., Luo, Q., Shiau, J., Wang, Y., Yuan, J., Sabri, S.M., Huang, S., Liao, C. Dynamic Behavior and Deformation of Calcareous Sand under Cyclic Loading. Soil Dynamics and Earthquake Engineering 2025. 199. Article no. 109730. DOI: 10.1016/j.soildyn.2025.109730
13. Kumar, S.S., Krishna, A.M., Dey, A. Parameters Influencing Dynamic Soil Properties: A Review Treatise. International Journal of Innovative Research in Science, Engineering and Technology. 2014. 3(4). Pp. 47–60.
14. Lekarp, F., Isacsson, U., Dawson, A. State of the Art. I: Resilient Response of Unbound Aggregates. Journal of Transportation Engineering, ASCE 2000. 126(1). Pp. 66–75. DOI: 10.1061/(ASCE)0733-947X(2000)126:1(66)
15. Li, D., Sussmann, T.R., Hyslip, J., Chrismer, S.M. Railway Geotechnics. Taylor and Francis Ltd. Boca Raton, 2016. 448 p.
16. Fattah, M.Y., Salim, N.M., Haleel, R.J. Liquefaction Potential of Sandy Soil from Small Laboratory Machine Foundation Model. International Review of Civil Engineering 2018. 9. Pp. 11–19.
17. Fattah, M.Y., Salim, N.M., Alwan, K.K. Contact Pressure Distribution under Circular Shallow Foundation Subjected to Vertical and Rocking Vibration Modes. Journal of Building Engineering 2019. 26. Article no. 100908. DOI: 10.1016/j.jobe.2019.100908
18. Abood, A.S., Fattah, M.Y., Al-Adili, A.S. Studying Characteristics and Strength of the Unsaturated Gypseous Soil with Various Saturation Degrees. Engineering and Technology Journal 2023. 41 (11). Pp. 1309–1324. DOI: 10.30684/etj.2023.140119.1453
19. Abood, A.S., Fattah, M.Y., Al-Adili, A.S. Assessment of Shear Strength Characteristics of the Unsaturated Gypseous Soil at Various Saturation Degrees. Cogent Engineering. 2023. 10(2). Article no. 2283303. DOI: 10.1080/23311916.2023.2283303
20. Das, B.M., Ramana, G. V Principles of Soil Dynamics. 2nd ed. Cengage Learning. Stamford, 2011. 575 p.
21. Al-Gharbawi, A.S.A., Fattah, M.Y., Mahmood, M.R. Effect of Carbonation on the Collapse Potential of Magnesium Oxide Treated Gypseous Soil. International Journal of Engineering. 2022. 35(4). Pp. 706–714. DOI: 10.5829/IJE.2022.35.04A.10
22. Zidan, A.J., Hussein, M.A. Behavior of Square Footing Subjected to Gypseous Soil under Eccentricity-Inclined Load. Journal of Tikrit of the Engineering Sciences. 2013. 20. Pp. 1–15.
23. Salih, N.B. Field Models on Gypseous Soils Reinforced with Stone Columns Stabilized with Asphalt and Lime. Thesis for M.Sc. Baghdad. University of Technology, 2003.
24. Al-Mufty, A.A. Effect of Gypsum Dissolution on the Mechanical Behavior of Gypseous Soils. Ph.D. Thesis. University of Baghdad, 1997.

Information about the authors:

***Mohammed Fattah**, PhD*
ORCID: https://orcid.org/0000-0002-4356-651X
E-mail: 40011@uotechnology.edu.iq

Ahmed Abood,
E-mail: bce.20.32@grad.uotec

Mohanad Sabri, *PhD*
ORCID: https://orcid.org/0000-0003-3154-8207
E-mail: mohanad.m.sabri@gmail.com

Aqeel Al-Adili, *PhD*
E-mail: 40077@uotechnology.edu.iq

Received 23.09.2025. Approved after reviewing 02.01.2026. Accepted 03.02.2026.